nature communications

Article

https://doi.org/10.1038/s41467-024-53306-1

Reverse hierarchical DED assembly in the cFLIP-procaspase-8 and cFLIP-procaspase-8-FADD complexes

Received: 7 June 2024

Accepted: 9 October 2024

Published online: 17 October 2024

Check for updates

Chao-Yu Yang[1], Yi-Chun Tseng[1,2,5], Yi-Fan Tu[2,5], Bai-Jiun Kuo[2], Li-Chung Hsu[3,4], Chia-I Lien[3], You-Sheng Lin[3], Yin-Ting Wang[1], Yen-Chen Lu[2], Tsung-Wei Su[1], Yu-Chih Lo[2] ✉ & Su-Chang Lin[1] ✉

cFLIP, a master anti-apoptotic regulator, targets the FADD-induced DED complexes of procaspase-8 in death receptor and ripoptosome signaling pathways. Several tumor cells maintain relatively high levels of cFLIP in achieving their immortality. However, understanding the three-dimensional regulatory mechanism initiated or mediated by elevated levels of cFLIP has been limited by the absence of the atomic coordinates for cFLIP-induced DED complexes. Here we report the crystal plus cryo-EM structures to uncover an unconventional mechanism where cFLIP and procaspase-8 autonomously form a binary tandem DED complex, independent of FADD. This complex gains the ability to recruit FADD, thereby allosterically modulating cFLIP assembly and partially activating caspase-8 for RIPK1 cleavage. Our structure-guided mutagenesis experiments provide critical insights into these regulatory mechanisms, elucidating the resistance to apoptosis and necroptosis in achieving immortality. Finally, this research offers a unified model for the intricate bidirectional hierarchy-based processes using multiprotein helical assembly to govern cell fate decisions.

Death receptor (DR)-mediated signaling pathways are pivotal in determining cell fate, influencing embryogenesis, tissue development, homeostasis, and immune responses[1,2]. Two types of DRs initiate apoptotic complex formation via distinct mechanisms: Fas (CD95), DR4, or DR5 directly recruit Fas-associated death domain (FADD) through homotypic interactions between their death domain (DD), while tumor necrosis factor receptor 1 (TNFR1) recruits TNFR-associated DD (TRADD) and a DD kinase called receptor-interacting protein kinase 1 (RIPK1). Notably, RIPK1 participates not only in FADD-mediated apoptotic cascades but also in cell-survival pathways[3,4].

DR-mediated apoptotic signaling complex formation follows a hierarchical/sequential binding process[5]. After CD95 binds FADD, FADD uses its death-effector domain (DED) to bind procaspase-8 (Casp-8) and then cellular FLICE-inhibitory proteins (cFLIP), forming the death-inducing signaling complex (DISC) or complex I[6,7]. DISC would trigger apoptosis unless cFLIP levels inhibit full Casp-8 activation[8–12].

In TNFR1 signaling, TNFR1, TRADD, and RIPK1 form complex I for NF-κB activation[13–18], which then internalizes and releases RIPK1 to sequentially bind FADD, Casp-8, and cFLIP to form cytosolic complex IIa[19]. Complex IIa becomes antiapoptotic due to RIPK1-NF-κB-mediated upregulation of antiapoptotic proteins, such as cFLIP[17,19–25]. Cycloheximide (CHX) attenuates cFLIP upregulation, enabling TNF to induce apoptosis in Jurkat cells[26,27]. However, the structural basis for the regulatory mechanism of anti-apoptosis upon cFLIP upregulation remains inconclusive due to the lack of atomic coordinates to unveil the complex assembly induced by cFLIP.

[1]Genomics Research Center, Academia Sinica, Taipei 11529, Taiwan. [2]Department of Biotechnology and Bioindustry Sciences, College of Bioscience and Biotechnology, National Cheng Kung University, Tainan 70101, Taiwan. [3]Institute of Molecular Medicine, College of Medicine, National Taiwan University, Taipei 10002, Taiwan. [4]Center of Precision Medicine, College of Medicine, National Taiwan University, Taipei 10002, Taiwan. [5]These authors contributed equally: Yi-Chun Tseng, Yi-Fan Tu. ✉e-mail: gracelo@ncku.edu.tw; tomlin@gate.sinica.edu.tw

FADD-Casp-8-cFLIP-mediated signaling pathways are intricate and sometimes controversial. cFLIP was thought to inhibit cell death by targeting the FADD-Casp-8 subcomplex[7,28,29]. This resultant FADD-Casp-8-cFLIP subcomplex was believed to prevent full Casp-8 activation, inhibiting apoptosis[7,30,31]. It might also inhibit necroptosis by cleaving RIPK1 if cFLIP contains a pseudo-caspase domain[32]. However, the timing of FADD-Casp-8-cFLIP subcomplex formation in preventing RIPK1-mediated necroptosis is uncertain.

In TNFR1 signaling, the formation of the FADD-Casp-8 subcomplex is not only positioned downstream of RIPK1 but also dispensable for RIPK1-mediated necroptosis[33,34], raising questions about cFLIP's role when upregulated by TNF-induced RIPK1-mediated NF-κB activation. Alternatively, an immediate FADD-Casp-8-cFLIP subcomplex upon cFLIP upregulation might be required to prevent RIPK1-mediated necroptosis, warranting investigations with cFLIP overexpression.

The significance of FADD-Casp-8-cFLIP-containing complexes in inhibiting apoptosis and necroptosis is highlighted by embryonic lethality at E10.5 in mice lacking cFLIP, Casp-8, or FADD[35–37]. FADD or Casp-8 deficiency promotes TNF-induced RIPK1-dependent necroptosis[33,34], mediated by a complex known as the necrosome or complex IIc[38]. Both deficiencies are rescued by RIPK3 ablation, blocking necroptosis[32,39,40], whereas embryos lacking cFLIP and RIPK3 succumb to TNF-induced apoptosis[39].

Additionally, a FADD-Casp-8-cFLIP-containg complex that inhibits TLR/TRIF or interferons (IFN)-initiated necroptosis via RIPK1 is crucial for postnatal development and maintaining epithelial homeostasis[41,42]. A similar complex also regulates the activation of NLRP3 inflammosome[43–45]. Moreover, elevated cFLIP expression could sustain the survival or immortality of some tumor cells[7,28,44,46,47], be important for heart development, correlate with Rheumatoid Arthritis, Multiple sclerosis, and Diabetes mellitus[48], and regulate NLRP1b/NLRC4-induced apoptosis[49], suggesting the presence of a FADD-Casp-8-cFLIP subcomplex in certain cells, even without DR activation.

Existing models predict DED-driven assembly of FADD, Casp-8, and cFLIP in DR-mediated signaling[5,50–55]. Obtaining the atomic coordinates of the ternary complex faces challenges from self-aggregation/precipitation of overexpressed Casp-8 tandem DED (tDED)[51] and sample heterogeneity as the ratios of the three proteins to one another vary in different cells and conditions[5,50,52–54]. Recently, we used mutagenesis to trap a homogeneous ternary complex of full-length (referred to as FuL) wild-type (WT) FADD, WT cFLIP tDED, and Casp-8 tDED. We presented the atomic coordinates of the complex, proposing that FADD and Casp-8 assemble an intermediate complex, essential to the formation of a composite-binding site (CBS) and subsequent targeting by cFLIP or Casp-8 in regulating apoptosis[56].

In this work, we present the atomic coordinates of the binary cFLIP-Casp-8 tDED complexes and the ternary DED complexes with Casp-8 activation-defective FADD, uncovering an unexpected assembly process that occurs in reverse order. The structures reveal that cFLIP tDED could form a homo-double-layer intermediate complex to recruit Casp-8 tDED, autonomously generating a stable cFLIP-Casp-8 complex. This binary complex then recruits FADD, resulting in a ternary complex dubbed "the cFLIP-Casp-8-FADD complex." This discovery suggests a reverse hierarchical DED assembly mechanism, which may confer resistance to DR-mediated or DR-independent death signaling in tumor cells with elevated cFLIP levels. Furthermore, the process highlights the intricate, bidirectional nature of hierarchical assembly mechanisms employed by helical multiprotein DD-fold complexes in regulating cell fate determination.

Results

cFLIP tDED and Casp-8 tDED form a binary oligomeric complex

Previously, as we sought to understand how DED assembles the complexes involving cFLIP, Casp-8, and FADD in order to govern signaling[56], we encountered a challenge. Casp-8 tDED (Casp-8^{tDED}) filaments predominated upon overexpression in the absence of FADD, hindering multiprotein complex reconstitution.

To address this, we recently explored mutations aimed at reducing tDED self-filamentation while preserving Casp-8-cFLIP interaction. Specifically, we introduced mutations Casp-8 F122A (in DED2) and cFLIP H7G (in DED1), resulting in the mutants Casp-8^{tDED_F122A} (referred to as C8^{F122A}) and cFLIP^{tDED_H7G} (referred to as CF^{H7G}), respectively. Overexpressing these mutants not only generated C8^{F122A} filaments but also successfully led to the formation of a smaller, oligomeric complex C8^{F122A}-CF^{H7G}, independently of FADD[56].

In our quest for diffractive crystals and hence atomic coordinates to elucidate how cFLIP and Casp-8 form an oligomeric complex in the absence of FADD, we introduced double F122G/L123G mutations to further weaken Casp-8 tDED filamentation, reducing sample heterogeneity. This enabled us to trap and purify homogeneously the CF^{H7G}-C8^{FGLG} complex for crystallization (Fig. 1a, b). We determined its crystal structure at 2.1 Å resolution (Supplementary Table 1 and Supplementary Fig. 1a), which revealed a 6:4 stoichiometry based on the selenium atom positions (Fig. 1c; where CFf$_1$ denotes DED1 of cFLIP chain f, please see the figure legend of Fig. 1c for naming convention) and a helical assembly of the tDED complex (Supplementary Movie 1). Notably, the 2.1 Å atomic coordinates confirmed that cFLIP^{tDED} closely resembles other DEDs, except for the disordered H3 helices (Supplementary Fig. 1a; where ^{2}H4 denotes helix 4 of DED2). The sequence identity between any two DEDs is ranging from 16.2% to 34.1% (Supplementary Fig. 1c).

Significantly, in the binary CF^{H7G}-C8^{FGLG} complex, we observed six cFLIP tDED molecules (Fig. 1c), exceeding the four cFLIP tDED molecules documented in our previous ternary 3:3:4 FADD^{FuL}-C8^{FuL_FGLG_CADA}-CF complex (Fig. 1d, PDB: 8YBX[56]), which was reconstituted using full-length WT FADD, WT cFLIP tDED, and full-length Casp-8 with both FGLG mutations to curb self-filamentation and CADA mutations to prevent self-cleavage[56]. This conspicuous difference in the count of cFLIP tDED molecules prompted further inquiry into the binary CF-C8^{FGLG} complex to unveil the underlying mechanisms of CF-C8 assembly.

More cFLIP^{tDED} units in the binary than the ternary complex

To ascertain the quantity of wild-type (WT) cFLIP^{tDED} within the binary complex, we reconstituted and homogeneously purified a (WT) cFLIP^{tDED}-Casp-8^{tDED_FGLG} complex, referred to as the CF-C8^{FGLG} complex (Fig. 2a, b). Subsequently, we determined its crystal structure at 3.3 Å resolution (Supplementary Table 1 and Supplementary Fig. 1b), unveiling a 9:4 CF-C8^{FGLG} complex composition (Fig. 2c). The 9:4 configuration in the CF-C8^{FGLG} crystal structure agrees with our small-angle X-ray scattering (SAXS) results (Fig. 2d and Supplementary Fig. 2 and Supplementary Table 2), showing the similarity in shape between the complexes observed in the crystals and those in solution. These findings decisively establish that the binary complex harbors a greater number of WT cFLIP tDED units compared to the FADD-containing ternary complex, i.e., the 3:3:4 FADD^{FuL}-C8^{FuL_FGLG_CADA}-CF complex.

Notably, the apparent molecular weights of the CF-C8^{FGLG} and CF^{H7G}-C8^{FGLG} complexes within the crystals exceeded those estimated by multi-angle light scattering (MALS) conducted at lower protein concentrations (Figs. 1b and 2b). This discrepancy can be attributed to the concentration-dependent dissociation of end molecules, resulting not only in a mixture of smaller DD-fold complexes but also in an underestimation of the molecular mass, as previously observed in other studies[57,58]. Nevertheless, the MALS results (7:4-8:4 or 8:3-9:3, as shown in Fig. 2b) continue to support the observation that the binary CF-C8^{FGLG} complex contains a greater quantity of cFLIP^{tDED} than the ternary FADD^{FuL}-C8^{FuL_FGLG_CADA}-CF complex.

Furthermore, our complex reconstitution results reveal a noteworthy distinction. Unlike WT Casp-8^{tDED}, WT cFLIP^{tDED} does not display a propensity to self-assemble filaments upon overexpression,

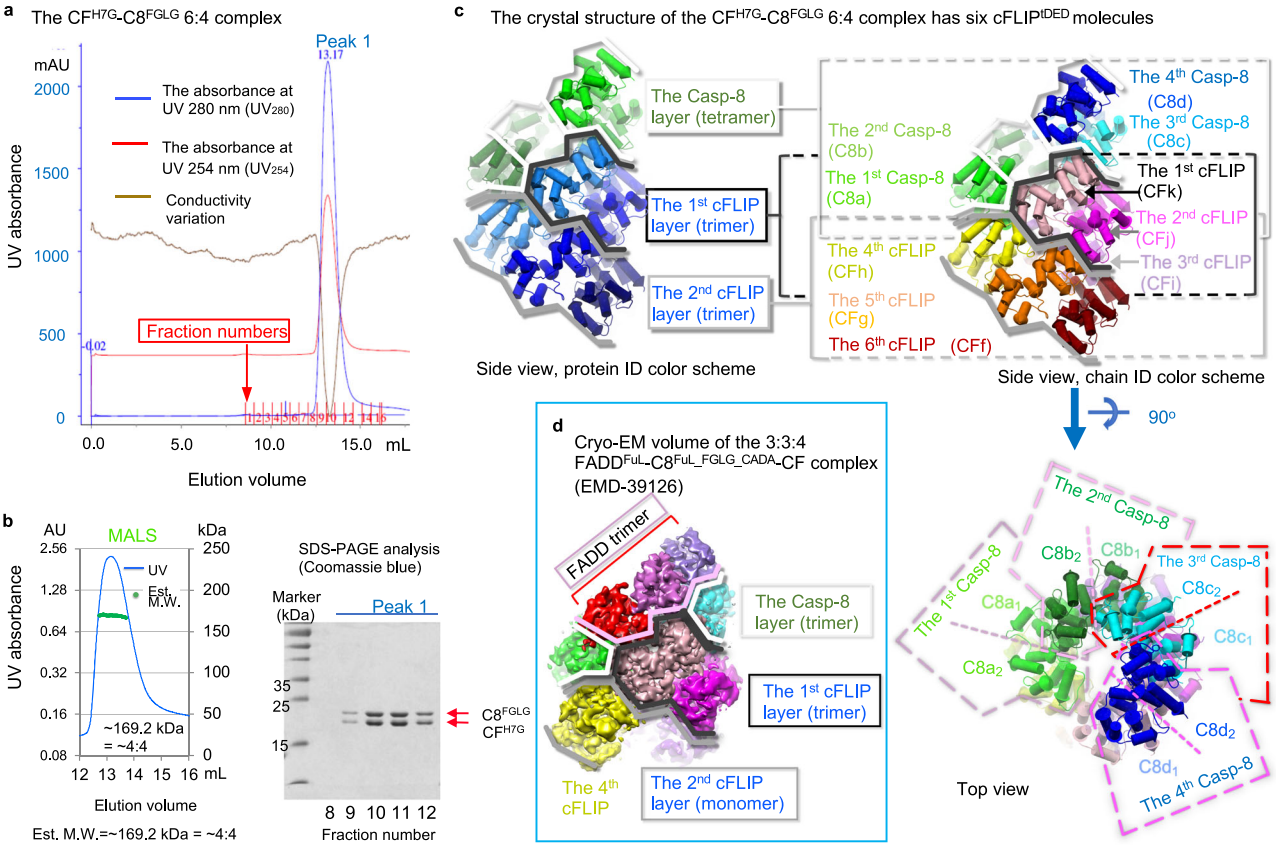

Fig. 1 | CF^H7G and C8^FGLG form a binary oligomeric complex in solution and crystals. a, b SEC-MALS analysis of the binary CF^H7G-C8^FGLG complex, with corresponding SDS-PAGE analysis in (**b**) for the peak fractions in (**a**). These results demonstrate that cFLIP^tDED and Casp-8^tDED form an oligomeric complex in solution. The MALS data suggests that the complex is smaller in solution than in crystals, indicating that the end molecules, likely cFLIP^tDED, have high dissociation constants similar to the DD complex[58]. Est. M.W., estimated molecular weight. The experiments were repeated twice with similar results. Source data are provided as a Source Data file. **c** The pipes-and-planks diagrams illustrate the crystal structure of the binary CF^H7G-C8^FGLG complex from different perspectives. In the protein ID color scheme of Figs. 1–3, Casp-8 and cFLIP are colored in different shades of green and blue, respectively, while in the chain ID color scheme, the molecules in Figs. 1–3 are colored as their counterparts in Fig. 3g. Additionally, the C8^FGLG layer/tetramer, the 1st CF^H7G layer/trimer, and the 2nd CF^H7G layer/trimer are consistently highlighted by white, dark gray, and gray lines, respectively. C8d$_1$ and C8d$_2$ denote DED1 and DED2 of Casp-8^tDED chain d, respectively, while CFf represents cFLIP^tDED chain f. The dashed boxes in the top view indicate the positions of Casp-8 molecules as well as the DED1 and DED2 domains. **d** Depicts the cryo-EM volume of our previous ternary 3:3:4 FADD^FuL-C8^FuL_FGLG_CADA-CF complex for comparison (EMDB: EMD-39126)[56]. The FADD trimer is highlighted by pink lines, while the C8^FGLG trimer is highlighted by white lines.

particularly in the presence of Casp-8^tDED FGLG mutants. Instead, WT cFLIP^tDED demonstrates a preference for forming an oligomeric complex with C8^FGLG in overexpression studies.

The composite binding site in forming the 3rd cFLIP layer

Compared to the 9:4 CF-C8^FGLG complex, it is likely that the 6:4 CF^H7G-C8^FGLG complex represents a preceding, stable seeding complex. The atomic coordinates of the 6:4 CF^H7G-C8^FGLG complex (Fig. 3a) reveal that the complex comprises two cFLIP^tDED trimers, referred to as the "1st cFLIP layer" and "2nd cFLIP layer" (Fig. 3a–g and Supplementary Movie 2), located at the bottom end of the C8^FGLG layer/tetramer. In contrast, the atomic coordinates of the 9:4 CF-C8^FGLG complex (Fig. 3b), WT cFLIP^tDED assembles into three cFLIP^tDED trimers, with the third trimer designated as the "3rd cFLIP layer/trimer" at the bottom end (Fig. 3c–g). cFLIP^tDED in each layer assembles into similar trimers along the type III connectivity (Fig. 3g) via the type III-II-III composite self-assembling site (CSS)[56,59] (Fig. 3g and Supplementary Fig. 3), comprising one type II and two type III interfaces (Supplementary Fig. 3).

The observation of type III-II-III CSS-mediated cFLIP^tDED trimers in Fig. 3c–g aligns with our identification of the type III-II-III CSS-mediated Casp-8^tDED trimer in our previous 3:3:4 FADD^FuL-C8^FuL_FGLG_CADA-CF structure (Fig. 3d, PDB: 8YBX[56]). While the type III-II-III CSS-mediated Casp-8^tDED trimer could be considered the asymmetric unit of the Casp-8 filaments, the role of the type III-II-III CSS extends beyond the formation of a transient Casp-8^tDED trimer, interacting with composite binding site (CBS) that governs the assembly of the Casp-8 tDED filament and sequentially appears on the filament[56]. Therefore, the 6:4 CF-C8^FGLG complex may utilize CBS in governing the assembly the 3rd cFLIP layer of the 9:4 CF-C8^FGLG complex (Fig. 3g).

By comparing the atomic coordinates of the 6:4 CF^H7G-C8^FGLG (Fig. 3a) and 9:4 CF-C8^FGLG complexes (Fig. 3b), the CBS responsible for recruiting the first cFLIP^tDED (CFo) of the 3rd cFLIP layer could be identified (Orange lines in Fig. 3e–g and Supplementary Movie 3). The smaller size of the 6:4 CF^H7G-C8^FGLG complex could be attributed to the H7G mutation altering the type Ia surface of CF^H7G DED1 and hence impairing the CFo-binding CBS (Orange lines in Fig. 3f and Supplementary Fig. 3c). Therefore, our structures argue that the 6:4 CF^H7G-C8^FGLG complex could represent a minimal binary tDED complex trapped by cFLIP H7G and Casp-8 FGLG mutations. Additionally, two type III-II-III CSS-mediated cFLIP trimers form an intermediate complex of a cFLIP double layer (Fig. 3g), creating the CBS for recruiting cFLIP^tDED CFo in generating the 3rd cFLIP layer.

cFLIP^tDED double-layer intermediate complex binds Casp-8^tDED

Sequential CBS formation is a general concept that could also be used to reasonably explain how a DD, such as MyD88 DD, assembles an

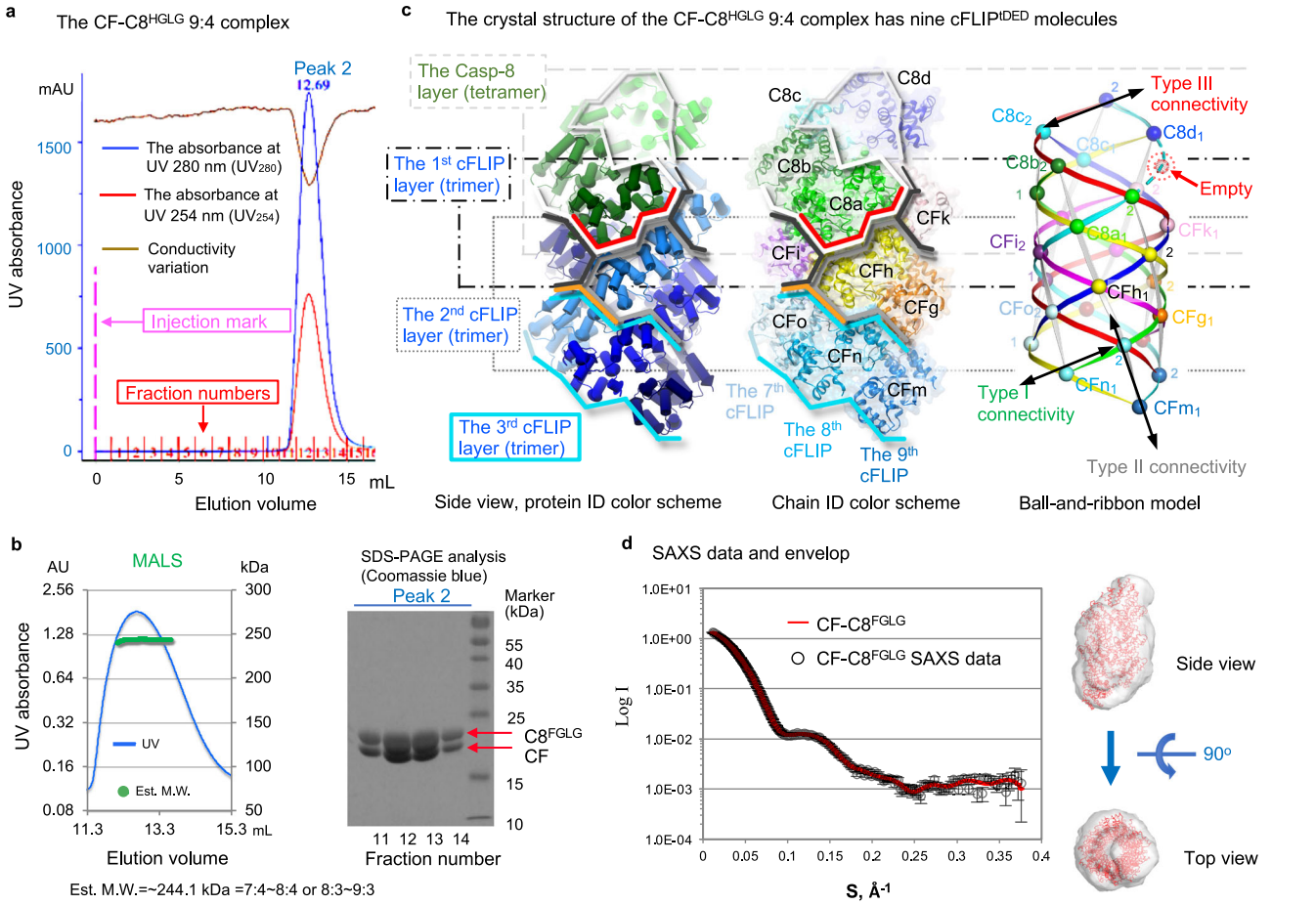

Fig. 2 | The binary complex has more WT CF molecules than the ternary complex. a, b SEC-MALS analysis of the binary CF-C8^{FGLG} complex, with corresponding SDS-PAGE analysis in (**b**) for the peak fractions in (**a**). The experiments were repeated twice with similar results. Source data are provided as a Source Data file. **c** The pipes-and-planks and ribbon diagrams illustrate the crystal structure of the binary CF-C8^{FGLG} complex. The C8^{FGLG} layer/tetramer and the 1st, 2nd, and 3rd WT CF layers/trimers are highlighted by white, dark gray, gray, and cyan lines, respectively, while the CBS for binding the cFLIP molecule CFo and the Casp-8 molecule C8a are highlighted by orange and red lines, respectively. The ball-and-ribbon diagram depicts the spatial relationship of individual DEDs with the type I, II, and III connectivity, represented by ribbons generated by the PyMOL program version 1.8.2.1, connecting the spatially conserved Cα atoms of every two adjacent DEDs. Each conserved Cα atom, representing DEDs, is shown as a ball, including those of Casp-8 residues L62 and L162, and cFLIP residues L55 and L152. A red arrow indicates a space left by the absence of FADD DED, predicted as a dashed ball. Please note that all the spatially conserved tDEDs in different representations, including ribbons, balls, and hexagons, in different Figs., would receive the same chain ID and color. Please refer to the legend of Fig. 1c for details on the molecular color schemes used. C8d$_1$ denotes DED1 of Casp-8^{tDED} chain d, while CFf represents cFLIP^{tDED} chain f. **d** The crystal structure of the CF-C8^{FGLG} complex exhibits a size and shape comparable to the envelop derived from the SAXS data of the same complex.

intermediate complex to bind a different DD, such as IRAK4 DD, for subsequent complex extension[60]. Presumably, cFLIP preferentially targets the FADD-Casp-8 complex to form a non-apoptotic ternary complex[7,28,29]. Recently, we reported the ternary 3:3:4 FADD^{FuL}-C8^{FuL_FGLG_CADA}-CF structure (PDB: 8YBX[56]), suggesting that WT cFLIP tDED preferentially targets the CBS on the binary 3:3 FADD-Casp-8 intermediate complex, highlighted by orange lines in Fig. 3d, and subsequently assembles a tetramer in blocking apoptotic signaling[56].

However, due to the absence of FADD, the binary 9:4 CF-C8^{FGLG} structure lacks the CBS found in the binary 3:3 FADD-Casp-8 intermediate complex. The absence of FADD leaves a space and an incomplete CBS on the C8^{FGLG} tetramer (Supplementary Movie 4), which are highlighted, respectively, by a red arrow and orange lines/dotted lines in Fig. 3b. It is very likely that the incomplete CBS on the C8^{FGLG} tetramer is unable to recruit the first cFLIP^{tDED} (CFk) of the 1st cFLIP layer to initiate the formation of the binary complex (Fig. 3g).

Alternatively, to achieve sequential CBS formation for assembling a binary complex, the presence of a cFLIP^{tDED} double layer in the 6:4 CF^{H7G}-C8^{FGLG} structure argues that cFLIP^{tDED} self-assembles an intermediate complex of double layer, creating a CBS (red lines in Fig. 3e–g) for binding the first Casp-8^{tDED} (C8a) (Supplementary Movie 5). Subsequently, four Casp-8^{tDED} molecules were recruited, completing the 6:4 binary complex (Fig. 3a–g). It is likely that WT cFLIP^{tDED} also utilizes the same mechanism to recruit four Casp-8^{tDED} molecules, resulting in the 9:4 CF-C8^{FGLG} complex (Fig. 3g).

Taken together, the similarities and differences between the atomic coordinates of the 6:4 CF^{H7G}-C8^{FGLG} and 9:4 CF-C8^{FGLG} complexes suggest that cFLIP^{tDED} could assemble a double-layer intermediate complex possessing two CBS with different specificities. One located on the top end binds Casp-8^{tDED} (Red lines in Figs. 2c, and 3b, e–g, and i), while the other, located on the bottom end, binds cFLIP^{tDED} (Orange lines in Fig. 3e–g and Supplementary Fig. 3c), as described above. The atomic coordinates of the binary complexes unveil previously undiscovered characteristics of cFLIP tDED, apparently different from the characteristics whereby cFLIP tDED preferentially targets the CBS of the FADD-Casp-8 DED intermediate complex, as unveiled by the atomic coordinates of our previous ternary 3:3:4 FADD^{FuL}-C8^{FuL_FGLG_CADA}-CF complex (PDB: 8YBX[56]), in blocking DR-mediated apoptotic signaling.

https://doi.org/10.1038/s41467-024-53306-1

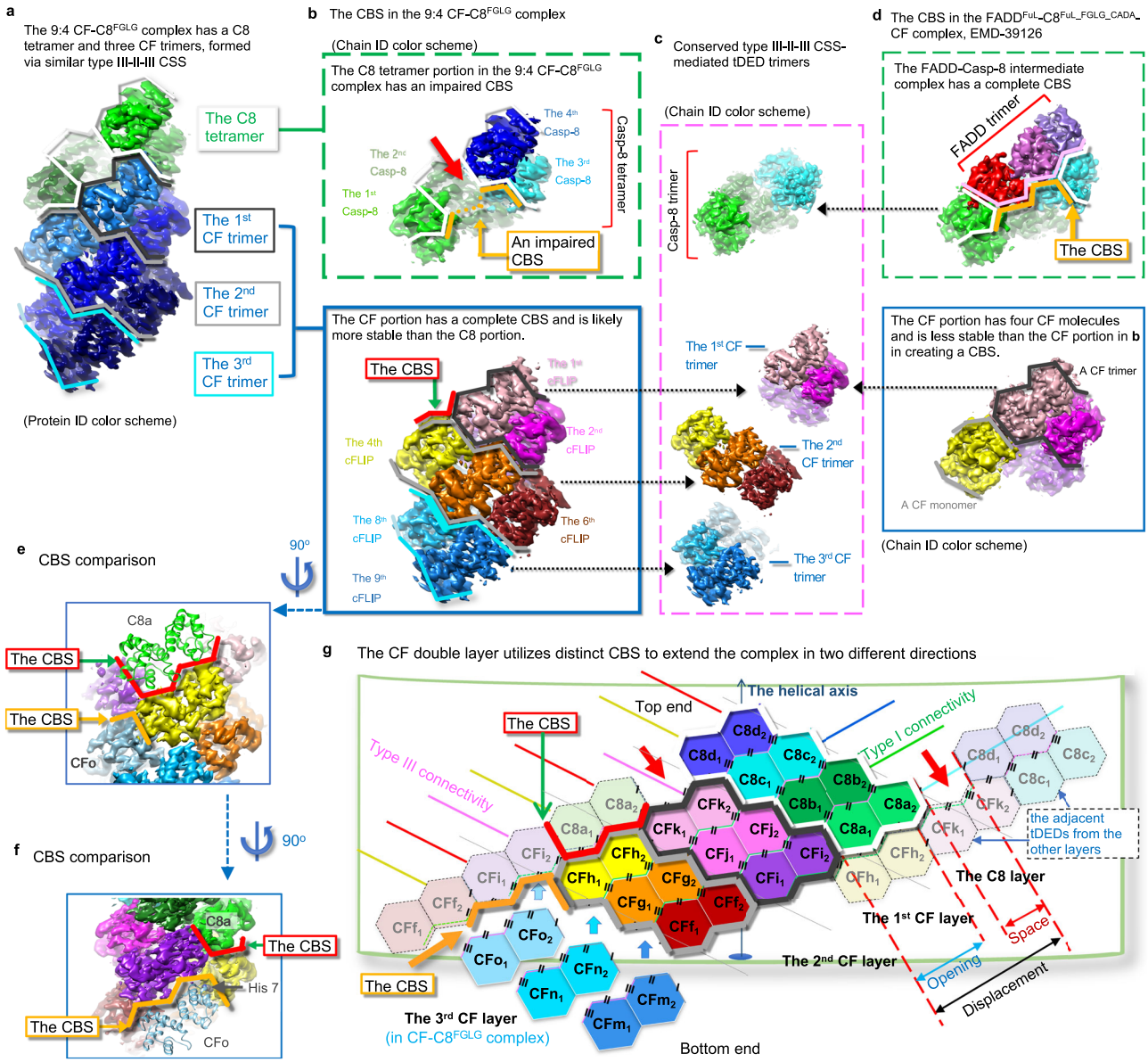

Fig. 3 | cFLIP^{tDED} double-layer intermediate complex utilizes different CBS to recruit Casp-8^{tDED} and cFLIP^{tDED}. **a** Crystal structure of the binary CF-C8^{FGLG} complex. Please refer to the legend of Fig. 1c for details on the molecular color schemes used. **b** Different CBS in the binary CF-C8^{FGLG} complex. The green dashed box shows the C8 tetramer portion, while the blue box shows the CF portion. Orange lines highlight the impaired CBS on the C8^{FGLG} tetramer due to a space, indicated by a red arrow, created by the absence of FADD DED. Red lines indicate the potential CBS on the WT CF double-layer intermediate complex. The CF and C8^{FGLG} portions are separated for clarity in visualizing the CBS. **c** Displays the conserved type III-II-III CSS-mediated CF and C8^{FGLG} trimers from (**b**) and (**d**), respectively. Molecules with the same chain ID in (**b**) to (**d**) are oriented similarly. **d** The green dashed box highlights the CBS, represented by orange lines, on the FADD-Casp-8 intermediate complex of our previous ternary complex in Fig. 1d for comparing with the CBS in (**b**). For clarity, the FADD-C8^{FGLG} and CF portions are separated. The CF portion is in the blue box. **e**, **f** Red lines and orange lines highlight the CBS for the Casp-8 molecule C8a and the cFLIP molecule CFo, respectively, on the WT CF double-layer intermediate complex in (**b**), viewed from different angles. **g** 2D representation of the binary complexes illustrates distinct CBS, extending the complex along the C8 (top) end and CF (bottom) end. A notable distinction between the CF^{H7G}-C8^{FGLG} and CF-C8^{FGLG} complexes is the presence of additional cFLIP^{tDED} molecules CFo, CFm, and CFn in the latter. Each hexagon represents a DED domain, while the dashed ones represent the adjacent tDEDs from the other layers. As in (**b**), a red arrow indicates a space created by the absence of FADD DED. Red lines and orange lines highlight different CBS described in (**e**) and (**f**). Pink and green angled lines are detailed in Supplementary Fig. 3. C8d$_1$ denotes DED1 of Casp-8^{tDED} chain d, while CFf represents cFLIP^{tDED} chain (**f**).

cFLIP self-assembly is crucial to binary complex formation

To identify important residues involved in the formation of minimal binary tDED complex, we introduced additional mutations on different interfaces of the CF^{H7G} mutant and assessed their ability to interact with the C8^{FGLG} mutant through pulldown experiments. Two types of interface residues were targeted for mutagenesis. One type, referred to as “type a” surface residues, is solely involved in cFLIP^{tDED} self-assembly. The mutations include a type Ia mutation, R38D, two type IIa mutations, E46A and K140D, and two type IIIa mutations, D31A and K124D (Fig. 4a, interfaces 1, 2, 4, 3, and 5, respectively). The other type, referred to as “type b” surface residues, participates in both cFLIP^{tDED} self-assembly and CF-C8^{FGLG} interaction. The mutations include a type Ib mutation, F114A, and two type IIb mutations, K69D and I162A (Interfaces 6, 7, and 9, respectively, in Fig. 4b and also interfaces 1, 4, and 2 in Fig. 4a). In addition, the mutations include two type IIIb mutations, E11A and R70D, on both interface 10 in Fig. 4b and interface 3 in Fig. 4a, as well as two type IIIb mutations, E102A and D105A, on both interface 8 in Fig. 4b and interface 5 in Fig. 4a. The mutagenesis

https://doi.org/10.1038/s41467-024-53306-1

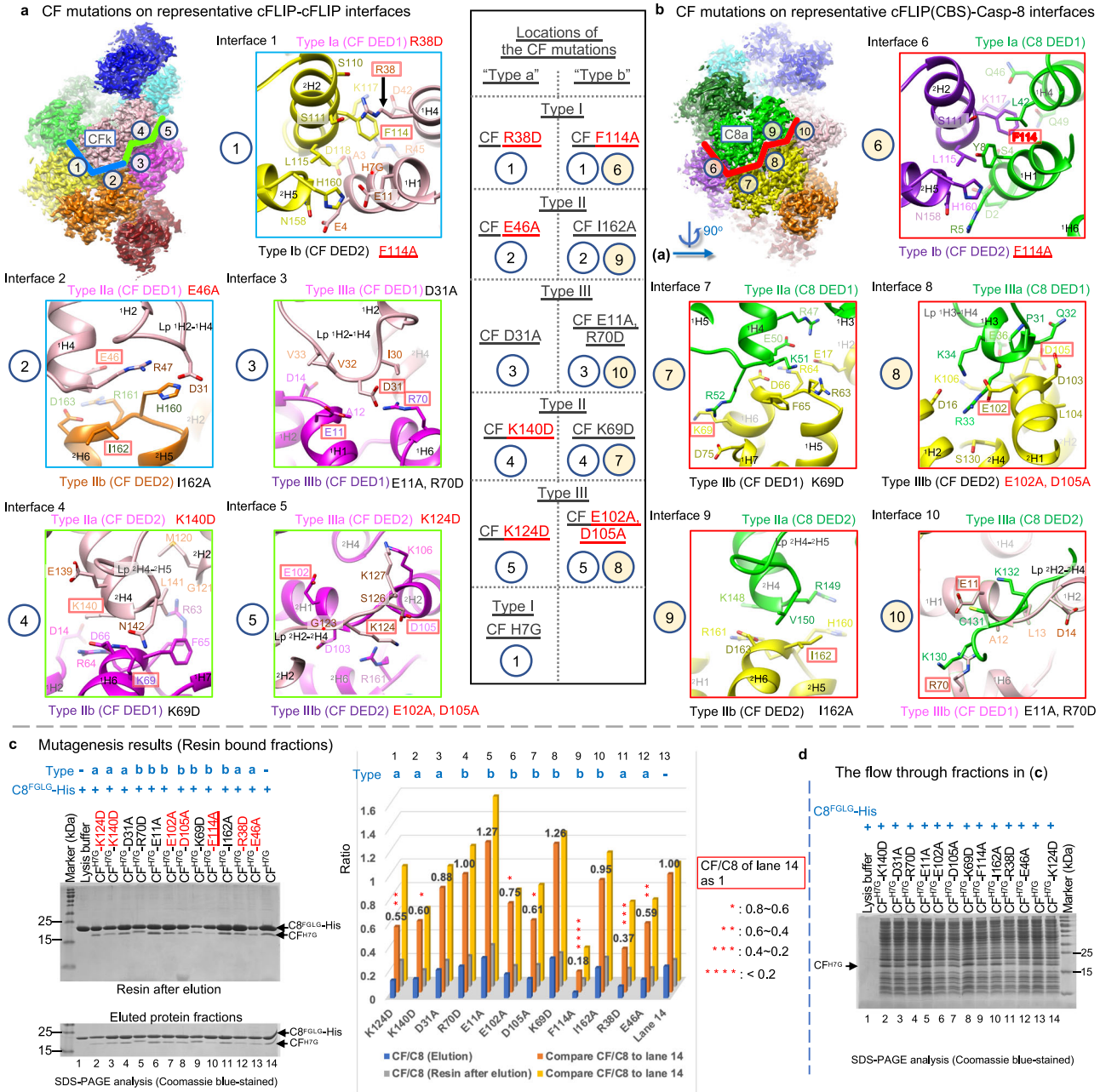

Fig. 4 | cFLIP^{tDED} self-assembly is crucial for the formation of the CF^{H7G}-C8^{FGLG} complex. a Illustration of five representative interfaces involved in the cFLIP-cFLIP interaction in the CF^{H7G}-C8^{FGLG} complex. Interface residues and the cFLIP mutations generated in this study are depicted. Thick green lines highlight the type III-II-III interface, while thick blue lines highlight the representative interfaces between two type III-II-III CSS-mediated cFLIP^{tDED} trimers. Residues used in mutagenesis studies are highlighted with red boxes, while glycine residues are indicated by red dots. 'Lp' denotes loop regions. The list in the black box outlines the positions of CF mutations on the surfaces displayed in (**a**) and (**b**). The molecules are colored as their counterparts in Fig. 3g. **b** Illustration of five interfaces involved in the interaction between the cFLIP double-layer intermediate complex and Casp-8 within the same complex. Thick red lines highlight the Casp-8-recruiting CBS on the cFLIP double-layer intermediate complex. Interface residues and the cFLIP mutations generated in this study are depicted. **c** Pulldown assay of CF^{H7G} and mutant CF^{H7G} by His-tagged C8^{FGLG} demonstrating the importance of cFLIP^{tDED} self-assembly in the formation of the binary complex. Resin-bound fractions are divided into the eluted protein fractions and the resin after elution fractions, each analyzed by SDS-PAGE to assess the amount of bound CF and His-tagged C8^{FGLG}. Protein bands were quantified using ImageJ version 1.50i (https://imagej.net/ij/). The bar chart made by Excel version 16.54 shows the quantified mutagenesis results of (**c**) (therefore, $n = 1$), with the ratios of cFLIP to Casp-8 plotted as blue and light blue bars for the eluted protein and resin fractions after elution, respectively. Each ratio is normalized to that of lane 14, with normalized results plotted as orange and yellow bars, respectively, and the ratio indicated on top. "Type a" and "type b" cFLIP mutations are indicated. **d** SDS-PAGE analysis result of the flow through fractions from (**c**). The experiments of (**c**) and (**d**) were repeated twice with similar results. Source data are provided as a Source Data file.

results indicate that additional R38D (type Ia), E46A (type IIa), K140D (type IIa), K124D (type IIIa), F114A (type Ib), and E102A/D105A (type IIIb) mutations on the CF^{H7G} mutant could impaired the CF^{H7G}-C8^{FGLG} interaction (Fig. 4c, d).

Since "type a" surface residues of cFLIP^{tDED} are involved only in cFLIP^{tDED} self-assembly in the binary 6:4 CF^{H7G}-C8^{FGLG} structures, impaired CF^{H7G}-C8^{FGLG} interactions by "type a" mutations K124D, K140D, R38D, and E46A (Fig. 4c, lanes 2, 3, 12, and 13 and columns 1, 2, 11, and 12, respectively) suggest that cFLIP^{tDED} self-assembly is crucial for CF^{H7G}-C8^{FGLG} interaction in the pulldown experiments. Therefore, a double-layer intermediate complex observed in the binary 6:4 CF^{H7G}-C8^{FGLG} structures is probably required for cFLIP^{tDED} to stably bind C8^{FGLG}

in this setting. Based on the atomic coordinates, these mutagenesis results support the idea that the type IIIa and IIa surfaces of cFLIP DED2 (Fig. 4a, interfaces 5 and 4, respectively), and the type Ia and IIa surfaces of cFLIP DED1 (Fig. 4a, interfaces 1 and 2, respectively) could directly mediate the formation of the CF^{H7G} double-layer intermediate complex and hence indirectly regulate CF^{H7G}-$C8^{FGLG}$ interaction.

"Type b" surface mutations of $cFLIP^{tDED}$ could have two different effects, $cFLIP^{tDED}$ self-assembly and CF-$C8^{FGLG}$ interaction. We found that introducing E102A, D105A, and F114A to the CF^{H7G} mutant impaired CF^{H7G}-$C8^{FGLG}$ interaction (Fig. 4c, lanes 7, 8, and 10, and columns 6, 7, and 9, respectively). Notably, cFLIP residue F114, belonging to the FL motif of DED2, is inserted into a pocket made by cFLIP residues A3, H7, R38 and D42 in type I $cFLIP^{tDED}$-$cFLIP^{tDED}$ interaction (Fig. 4a, interface 1) or a pocket made by Casp-8 residues S4, Y8, L42, and Q46 in type I CF-$C8^{FGLG}$ interaction (Fig. 4b, interface 6). Since the H7G mutation on cFLIP tDED attenuates its self-assembly (Fig. 3f), resulting in a smaller, 6:4 CF^{H7G}-$C8^{FGLG}$ complex, the observation that F144A mutation (Fig. 4c, lane 10 and column 9) impaired the CF^{H7G}-$C8^{FGLG}$ interaction more significantly than E102A and D105A mutations could be attributed to the double F144A and H7G mutations affecting both the FL motif and interacting pocket on the type I interface involved in assembling the CF^{H7G} double-layer intermediate complex.

Minor Casp-8 tDED self-assembly in binary complex formation

To identify $Casp\text{-}8^{tDED}$ residues involved in the formation of minimal binary tDED complex, we introduced additional mutations on different interfaces of the $C8^{FGLG}$ mutant and assessed their ability to interact with the CF^{H7G} mutant. Like cFLIP tDED, there are two different types of Casp-8 tDED surface residues for mutagenesis. However, unlike cFLIP tDED, the "type a" surface residues Y8, R33, R52, K130, and K148 are involved in both $Casp\text{-}8^{tDED}$ self-assembly and CF^{H7G} interaction (Supplementary Fig. 4a, b), while the "type b" surface residues, including E12, N70, and E110, are involved only in $Casp\text{-}8^{tDED}$ self-assembly (Supplementary Fig. 4a). The mutagenesis results show that "type a" surface mutations K148D (type IIa, DED2), R33D (type IIIa, DED1), and R52D (type IIa, DED1) could impair CF^{H7G}-$C8^{FGLG}$ interaction (Supplementary Fig. 4c, lanes 5, 8, and 9 (columns 4, 7, and 8), respectively).

Casp-8 Y8A, R52E, F122G/L123G and K148D/R149E mutations were known to impair the formation of apoptotic Casp-8 death effector filament (DEF)[51,53], in which Y8A, R52E, and K148D/R149E belong to "type a" surface mutations, while F122G/L123G belong to "type b" mutations. Since F122G/L123G double mutations impaired $C8^{FGLG}$ self-assembly[56], impaired CF^{H7G}-$C8^{FGLG}$ interaction observed in our mutagenesis results using additional "type a" surface mutations R33D, R52D, and K148D could be attributed to reduced $Casp\text{-}8^{tDED}$'s affinity to $cFLIP^{tDED}$. In contrast, additional "type b" surface mutations E12A, N70A, and E110A still retain CF^{H7G}-$C8^{FGLG}$ interaction (Supplementary Fig. 4c, lanes 7, 6, and 4 (columns 6, 5, and 3), respectively). Therefore, "type b" surfaces involved in Casp-8 tDED self-assembly play a less significant role in the binary tDED complex formation than other surfaces.

The binary CF^{H7G}-$C8^{FGLG}$ complex could bind FADD

The conventional understanding dictates that FADD initiates the recruitment of Casp-8, which subsequently leads to cFLIP recruitment, ultimately forming a ternary complex through a hierarchical binding process[5]. However, the purification of both the binary CF-$C8^{FGLG}$ and CF^{H7G}-$C8^{FGLG}$ complexes, along with mutagenesis results, suggest an alternative binding mechanism, operating in reverse order. In this scenario, $cFLIP^{tDED}$ first assembles a double-layer intermediate complex, utilizing a CBS to subsequently recruit $Casp\text{-}8^{tDED}$. Notably, examination of the binary complex structures reveals that the absence of FADD left an empty space (Figs. 2c and 3b, f), which would be occupied by FADD in the ternary 1:5:4 $FADD^{FuL\_H9G}$-$C8^{FGLG}$-CF^{H7G} complex (PDB: 8YD8[56]). This observation raises the intriguing possibility of a pre-assembled CF^{H7G}-$C8^{FGLG}$ complex binding FADD afterward, thus completing a hierarchical binding process in reverse order, a phenomenon we term the "reverse hierarchical binding process."

To investigate this possibility, we employed the CF^{H7G}-$C8^{FGLG}$ complex, purified after the removal of its His-tag, for pulldown experiments, assessing its interaction with a His-tagged, full-length FADD (Fig. 5a, b). Notably, the FADD used also contained a F25Y mutation ($FADD^{FuL\_F25Y}$), known to mitigate FADD aggregation without affecting Casp-8 interaction[61]. SDS-PAGE analysis revealed that the purified CF^{H7G}-$C8^{FGLG}$ complex, lacking the His-tag, indeed interacted with the FADD F25Y mutant (Fig. 5b, lanes 7 and 6), but not with the resin alone (Fig. 5b, lanes 4 and 3). Subsequently, the resultant ternary complex was successfully eluted and purified as a single peak (Fig. 5c, d). Moreover, electron microscopy imaging of the purified ternary complex revealed a globular shape, reminiscent of the crystal structure of the binary complex (Fig. 5e). These results strongly suggest that the generation of the ternary cFLIP-Casp-8-FADD complex can be done in reverse order, lending support to the hypothesis of a "reverse hierarchical binding process".

cFLIP recruits Casp-8 and then binds FADD in reverse order

We further utilized the FADD F25G mutant, which is known to be monomeric and inactive in Casp-8 activation[61,62], to reconstitute the ternary complex through co-purification. This approach helped us sidestep the formation of the complex via a hierarchical binding process. This choice was made because overexpressed WT FADD could trigger the formation of a ternary FADD-Casp-8-cFLIP DED complex[56], while the FADD F25Y mutant, capable of interacting with Casp-8 and inducing apoptosis[61,62], likely behaves similarly to WT FADD. In our co-purification experiments, we employed the full-length, inactive FADD F25G mutant ($FADD^{FuL\_F25G}$), a full-length Casp-8 mutant with catalytic inactivity and processing deficiency ($Casp\text{-}8^{FuL\_F122G/L123G/C360A/D374A/D384A}$), and wild-type $cFLIP^{tDED}$. This approach successfully yielded the ternary $cFLIP^{tDED}$-$Casp\text{-}8^{FuL\_F122G/L123G/C360A/D374A/D384A}$-$FADD^{FuL\_F25G}$ complex, designated as the CF-$C8^{FuL\_FGLG\_CADA}$-FA^{FuL_F25G} complex (Fig. 5f, g). These findings confirm that the binary CF-$C8^{FuL\_FGLG\_CADA}$ complex can indeed recruit the inactive FADD F25G mutant (Fig. 5g), further supporting the concept of a hypothetical "reverse hierarchical binding process".

To gain structural insight into this process, we treated the purified ternary complex protein with Bis-sulfosuccinimidyl suberate (BS3) crosslinker for cryo-EM studies. Subsequently, we solved the cryo-EM structure of the ternary complex (Supplementary Figs. 5 and 6), revealing the DED portion while the caspase domain of Casp-8 and the DD of FADD remained invisible. The structure and the resultant atomic coordinates of the ternary 5:3:3 CF-$C8^{FuL\_FGLG\_CADA}$-FA^{FuL_F25G} DED complex (also named Complex C, Fig. 5h and Supplementary Fig. 7a) were determined at a 3.7 Å resolution. The structure displayed three FADD F25G DED molecules arranged similarly to our previous 3:3:4 $FADD^{FuL}$-$C8^{FuL\_FGLG\_CADA}$-CF complex structure (PDB: 8YBX[56], Fig. 1d), rather than the 1:5:4 $FADD^{FuL\_H9G}$-$C8^{FGLG}$-CF^{H7G} complex structure (PDB: 8YD8[56]). The potential locations of the FADD DD were modeled using the previously determined full-length structure of FADD (PDB: 2GF5[63]) (Supplementary Fig. 7c). Notably, since FADD F25 mutation only affects the type I $FADD^{DED}$-$FADD^{DED}$ interaction (Fig. 6e and Supplementary Fig. 8b, interfaces 4 and 7) but not $FADD^{DED}$-$Casp\text{-}8^{tDED}$ and $FADD^{DED}$-$cFLIP^{tDED}$ interactions, the atomic coordinates (Fig. 5h, Complex C) confirm that $FADD^{DED\_F25G}$ is indeed recruited to the cFLIP-Casp-8 tDED complex in reverse order.

Early dissociation of FADD F25G yields binary byproducts

The DED portion of the 5:3:3 CF-$C8^{FuL\_FGLG\_CADA}$-FA^{FuL_F25G} complex contains fewer cFLIP DED molecules than its parental 9:4 CF-$C8^{FGLG}$ complex (Fig. 5h vs Fig. 2c), suggesting that the binding of FADD F25G mutant to the 9:4 CF-$C8^{FGLG}$ complex induces a transition to a ternary complex product. This product could resemble the 3:3:4 $FADD^{FuL}$-

https://doi.org/10.1038/s41467-024-53306-1

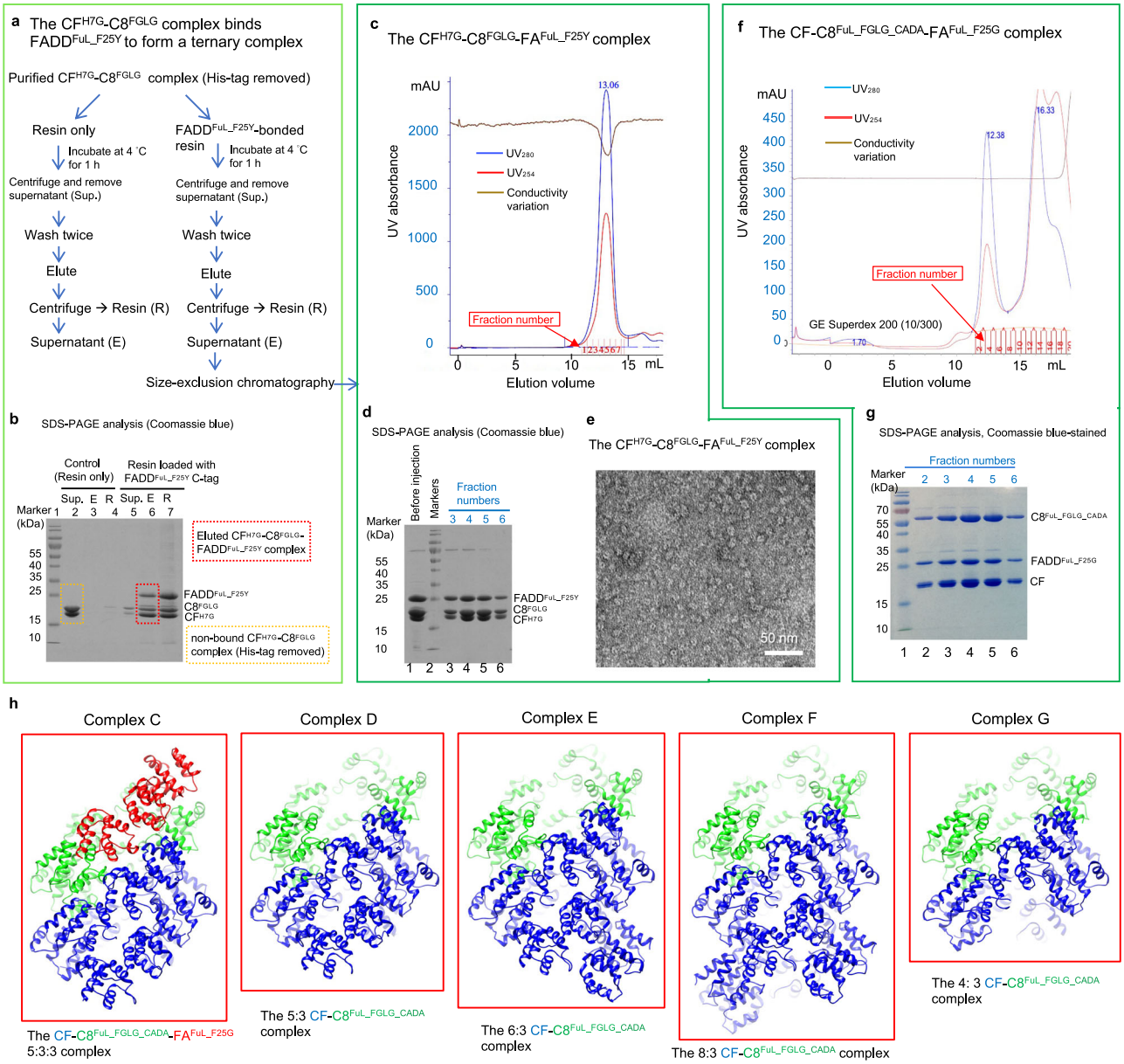

Fig. 5 | The binary CF^{H7G}-C8^{FGLG} complex binds FADD to form the ternary complex in reverse order. a Procedure of reconstituting the ternary CF^{H7G}-C8^{FGLG}-FA^{FuL_F25Y} complex in reverse order, utilizing resin-bound FADD^{FuL_F25Y} to pulldown tag-removed binary CF^{H7G}-C8^{FGLG} complex, with resin-only serving as a negative control. **b** SDS-PAGE analysis of the unbound supernatant fraction (Sup.), eluted bound protein fraction (E), and resin after elution (R) from (**a**). **c** Gel filtration profile of the ternary CF^{H7G}-C8^{FGLG}-FA^{FuL_F25Y} complex, using the sample from the eluted bound protein fraction (E) in (**a**) and (**b**), analyzed with a Superdex 200 increase (10/300 GL) column. **d** SDS-PAGE analysis of the peak fractions from (**c**). **e** Negative-stain electron microscopy (EM) analysis of the peak fractions in (**c**), demonstrating the globular shape of the ternary CF^{H7G}-C8^{FGLG}-FA^{FuL_F25Y} complex obtained in reverse order. Scale bar = 50 nm. **f** Gel filtration profile of the CF^{H7G}-C8^{FuL_FGLG_CADA}-FA^{FuL_F25G} complex obtained in reverse order following the procedure in (**a**). **g** SDS-PAGE analysis of the peak fractions from (**f**). The experiments of (**b**), (**d**), (**e**), and (**g**) were repeated twice with similar results. Source data are provided as a Source Data file. **h** Ribbon diagrams illustrating the atomic coordinates of five cryo-EM structures obtained from the cryo-EM sample of the CF^{H7G}-C8^{FuL_FGLG_CADA}-FA^{FuL_F25G} complex sample in (**f**). Blue, green, and red ribbons represent cFLIP, Casp-8, and FADD, respectively.

C8^{FuL_FGLG_CADA}-CF complex typically formed through a conventional hierarchical binding process.

Unexpectedly, from the same cryo-EM data set, we derived four additional binary tDED core structures with varied compositions through 3D reconstruction. These structures, termed Complexes D, E, F, and G, represent the 5:3, 6:3, 8:3 and 4:3 (WT)cFLIP^{tDED}-Casp-8^{tDED_FGLG} complexes, respectively, (Fig. 5h), solved at 3.6, 3.6, 3.5 and 4.0 Å resolution (Supplementary Figs. 5–7b). Notably, despite isolating the ternary complex with His-tagged FADD^{FuL_F25G}, approximately 80% of cryo-EM particles lacked FADD^{FuL_F25G} (Supplementary Fig. 5), aligning with prior observations of the mutant's weak binding affinity towards Casp-8 and cFLIP[61,62]. The appearance of the binary CF-C8^{FGLG} Complexes D to G supports the notion that FLIP and Casp-8 initially form a 9:4 CF-C8^{FGLG} complex before recruiting and hence being pulled down by His-tagged FADD^{FuL_F25G}. Importantly, the appearance of multiple structures in a cryo-EM data set also suggests a dynamic process was involved[64].

It is plausible that after the 9:4 cFLIP-Casp-8 binary complex binds to FADD, the resultant ternary complex undergoes a FADD-dependent transition. The observed binary CF-C8^{FGLG} Complexes D to G likely represent byproducts trapped after the early dissociation of FADD^{F25G} from the ternary complex during the transition to its final product.

https://doi.org/10.1038/s41467-024-53306-1

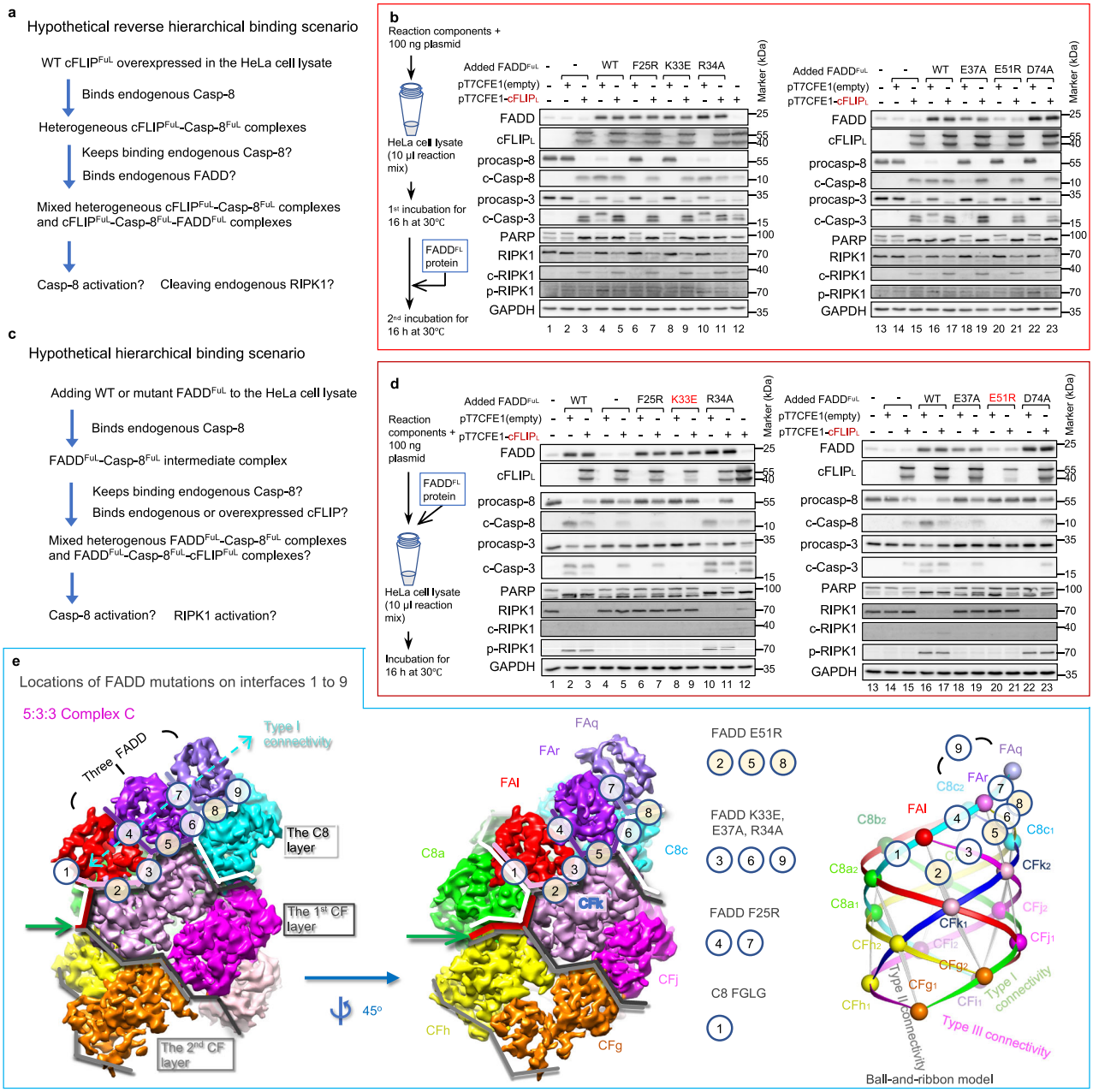

Fig. 6 | Expressed cFLIP inhibits FADD-induced Casp-8 activation but partially activates Casp-8. a Illustration of possible reactions in HeLa cell lysate under a hypothetical reverse hierarchical binding scenario. Overexpression of $cFLIP^{FuL}$ could trigger reverse binding by forming a binary complex with endogenous Casp-8, which can then recruit FADD. Possible biochemical reactions, demonstrated in (**c**) and (**d**), include partial Casp-8 activation and RIPK1 cleavage. **b** Illustration of possible reactions in HeLa cell lysate under a hypothetical hierarchical binding scenario. The addition of FADD protein could initiate the formation of an intermediate complex with endogenous Casp-8, which could then recruit either Casp-8 or cFLIP. Added FADD could also bind RIPK1. Possible biochemical reactions, demonstrated in (**c**) and (**d**), include full Casp-8 activation and RIPK1 activation. **c** Cell-lysate-based mutagenesis results. cFLIP-expressing or control plasmids were added to HeLa cell lysate for a 16-h incubation, followed by the addition of FADD protein for another 16-h incubation. Results were analyzed by western blotting. The western blotting data were repeated twice with similar results. **d** Cell-lysate-based mutagenesis results with simultaneous addition of cFLIP-expressing plasmids and FADD protein to HeLa cell lysate for a 16-h incubation. The effects of FADD mutations were examined by western blotting. Source data are provided as a Source Data file. **e** Illustration of seven interfaces between FADD and the binary CF-C8 sub-complex and two interfaces between adjacent FADD molecules in the triple-FADD 5:5:3 Complex C. The complex is shown as molecular surfaces using cryo-EM envelops and as a ball-and-ribbon model. Locations of various FADD mutations on different interfaces are indicated. Green arrows point to the CBS, illustrated by red lines, for recruiting Casp-8 molecule C8a. White and gray lines indicate the Casp-8 layer or cFLIP layers. Interface residues are shown in Supplementary Fig. 8b. The molecules are colored as their counterparts in Figs. 1d and 3g. $C8d_1$ denotes DED1 of $Casp\text{-}8^{tDED}$ chain d, while CFf represents $cFLIP^{tDED}$ chain (**f**).

Consequently, the number of cFLIP molecules in the binary Complexes D to G is lower than its parental 9:4 $CF\text{-}C8^{FGLG}$ complex (Fig. 5h vs Fig. 2c). Notably, the numbers of CF and especially $C8^{FGLG}$ molecules in the 5:3 and 4:3 $CF\text{-}C8^{FGLG}$ Complexes D and G are approaching those in the 5:3:3 ternary Complex C and our previous ternary 3:3:4 $FADD^{FuL}\text{-}C8^{FuL\_FGLG\_CADA}$-CF complex (PDB: 8YBX[56], Fig. 1d), the presumable final product. Therefore, the gradual reduction in the number of cFLIP molecules observed in the binary byproducts suggests the possibility of an additional mechanism regulating the number of cFLIP molecules in the ternary complex during the FADD-dependent

transition. One potential mechanism is that the binding of FADD to the CF-C8^{FGLG} complex may trigger a change in the CF-C8 assembly, leading to the release of cFLIP (further discussed below).

In conclusion, our X-ray, cryo-EM and mutagenesis results (Figs. 1–5) provide evidence for a previously unexplored reverse hierarchical binding process. This process involves cFLIP initially forming a complex with Casp-8, followed by binding to FADD. Subsequent recruitment of FADD triggers the release of cFLIP, leading to the formation of a ternary complex akin to those typically generated by the hierarchical binding process.

Expressed cFLIP induces reactions in the reverse hierarchy

If increased levels of cFLIP$_L$ can initiate the reverse hierarchical binding process, it is plausible that the resulting cFLIP$_L$ intermediate complex could engage endogenous procaspase-8, promoting their heterodimerization and subsequent Casp-8 activation (Fig. 6a), given that heterodimerization between cFLIP$_L$ and procaspase-8 is crucial for cFLIP$_L$-mediated Casp-8 activation[5,44,65–67]. Upon recruitment of FADD to the binary complex, additional reactions such as RIPK1 cleavage may occur. To substantiate our structural discoveries, we expressed wild-type full-length cFLIP$_L$ in HeLa cell lysate and evaluated procaspase-8 activation.

Indeed, after a 16-h incubation, cFLIP$_L$ expression in HeLa cell lysate led to Casp-8 activation and the cleavage of cFLIP$_L$ (Fig. 6d, lanes 5 and 15), likely facilitated by enhanced heterodimerization of cFLIP$_L$ and Casp-8 via the resulting CF-C8 binary complex. Importantly, the observed Casp-8 activation was not attributed to any pre-existing or spontaneously formed Casp-8-activating intermediate complexes in the cell lysate, as evidenced by the control experiment (Fig. 6b, lanes 1 and 2), where no Casp-8 activation was observed after a 32-h incubation. To confirm that the induced Casp-8 activation by expressed cFLIP$_L$ was mediated by its pseudo-caspase domain, we expressed the tDED of cFLIP$_L$ and found no Casp-8 activation after a 16-h incubation (Supplementary Fig. 8a, lane 3). These results suggest that expressed cFLIP$_L$ can initiate the reverse hierarchical binding process in vitro, which requires the pseudo-caspase domain of cFLIP$_L$ for Casp-8 activation.

After a 32-h incubation, elevated levels of cFLIP also led to the cleavage of RIPK1 (Fig. 6b, lanes 3 and 15). Given that RIPK1 cleavage in necroptosis inhibition relies on cFLIP-Casp-8 heterodimers[32], and the reintroduction of FADD into FADD-deficient Jurkat cells suppresses TNF-induced necrosis[34], it is likely that the observed RIPK1 cleavage is mediated by endogenous FADD. This occurs after FADD is recruited to the CF-C8 binary complex formed due to elevated levels of cFLIP$_L$. Notably, endogenous procaspase-8 in cells does not spontaneously form filaments or complexes with cFLIP or FADD to initiate Casp-8 activation, as demonstrated by the control experiments (Fig. 6b, lanes 1, 2, 13, and 14). Therefore, the observed Casp-8 activation, cleavage of cFLIP$_L$, and cleavage of RIPK1 following cFLIP$_L$ overexpression suggest that cFLIP$_L$ overexpression could indeed trigger the reverse hierarchical binding process, leading to the observed reactions in the reverse hierarchy.

Expressed cFLIP inhibits FADD-induced Casp-8 activation

Differences were noted in the reactions induced by added FADD and expressed cFLIP$_L$ in HeLa cell lysate. Adding WT FADD protein to the cell lysate was known to efficiently trigger Casp-8 activation via a hierarchical binding process[56]. In our control experiments, Casp-8 activation by added FADD appeared more efficient than that induced by expressed cFLIP$_L$ after a 16-h incubation (Fig. 6d, lanes 16 vs 15 or 2 vs 5). Moreover, added FADD, but not expressed cFLIP$_L$, induced RIPK1 phosphorylation (Fig. 6d, lanes 16 vs 15 or 2 vs 5). While both added FADD and expressed cFLIP$_L$ could induce RIPK1 cleavage (Fig. 6b, lanes 4 and 16 for added FADD; lanes 3 and 15 for expressed cFLIP$_L$), the cleavage induced by expressed cFLIP$_L$ became more pronounced following a 32-h incubation compared to a 16-h incubation (Fig. 6d, lanes 5 and 15).

The hierarchical and reverse hierarchical binding processes both involve FADD, cFLIP, and Casp-8, suggesting potential crosstalk between the two processes if both are activated simultaneously. To investigate this possibility, we supplemented cFLIP$_L$-expressing HeLa cell lysate with FADD proteins and evaluated procaspase-8 activation, cFLIP cleavage, and RIPK1 cleavage.

After adding WT FADD protein to the HeLa cell lysate already expressing cFLIP$_L$ for 16 h, followed by an additional 16-h incubation, we observed consistent patterns of cFLIP$_L$-induced Casp-8 activation, cFLIP$_L$ cleavage, and RIPK1 cleavage (Fig. 6b, lanes 5 and 17 vs lanes 3 and 15). The absence of crosstalk in this context suggests that the expressed cFLIP$_L$ likely depleted endogenous Casp-8, forming complexes to activate Casp-8.

To further investigate the interplay between the two opposing signaling cascades, we introduced FADD protein along with the cFLIP$_L$-expressing vector into HeLa cell lysate, followed by a 16-h incubation. We observed that expressed cFLIP$_L$ significantly attenuated the robust Casp-8 activation induced by added FADD, while RIPK1 phosphorylation remained unaffected (Fig. 6d, lanes 16 vs 17 or 2 vs 3). Substituting cFLIP^{tDED} for cFLIP$_L$ confirmed that cFLIP^{tDED} alone is capable of halting added-FADD-induced Casp-8 activation (Supplementary Fig. 8a, lanes 7 and 8 vs 6). These findings collectively suggest that expressed cFLIP suppresses added-FADD-induced Casp-8 activation without affecting RIPK1 activation. Moreover, the observed Casp-8 activation in Fig. 6d, lane 3 or 17, is likely attributed to expressed cFLIP$_L$ rather than added FADD.

Expressed-cFLIP-induced Casp-8 activation requires FADD

We further investigated the role of FADD surfaces in the expressed-cFLIP-induced binding process. We employed FADD mutants (F25R, K33E, E37A, E51R, and D74A) known to be defective in added-FADD-induced Casp-8 activation[56], and examined their impact on expressed-cFLIP-induced reactions. Residues K33, E37 (Fig. 6e and Supplementary Fig. 8b, interfaces 3, 6, and 9) and E51 (Fig. 6e and Supplementary Fig. 8b, interfaces 2, 5, and 8) are located on the "type a" surfaces of FADD DED, interacting with the "type b" surfaces of Casp-8^{tDED} and cFLIP^{tDED} in the triple-FADD 5:3:3 CF-C8^{FuL_FGLG_CADA}-FA^{FuL_F25G} complex. Meanwhile, residue F25 is located on the type Ib surface crucial for FADD^{DED}-FADD^{DED} interaction (Fig. 6e and Supplementary Fig. 8b, interfaces 4 and 7). Notably, residue D74 belongs to the type IIb surface used only in the 1:5:4 FADD^{FuL_H9G}-C8^{FGLG}-CF^{H7G} complex (PDB: 8YD8[56]), which is not involved in the assembly of triple-FADD 5:3:3 CF-C8^{FuL_FGLG_CADA}-FA^{FuL_F25G} complex. As an additional positive control, we included the FADD R34A mutant, which retains the ability to induce Casp-8 activation.

In the presence of WT FADD or the WT-mimicking R34A mutant, expressed cFLIP inhibits added-FADD-induced Casp-8 activation in HeLa cell lysate, while itself triggering limited Casp-8 activation (Fig. 6d, lanes 3 vs 2, and lanes 11 vs 10, respectively), as previously mentioned. As expected, adding Casp-8 activation-defective FADD mutants K33E and E51R to HeLa cell lysate failed to activate Casp-8 (Fig. 6d, lanes 8 and 20, respectively), yet these mutants also inhibited cFLIP$_L$-expression-induced Casp-8 activation (Fig. 6d, lanes 9 and 21, respectively). These findings suggest that cFLIP$_L$-expression-induced Casp-8 activation necessitates the presence of FADD, as well as FADD residues K33 and E51.

Importantly, while Casp-8 activation-defective FADD mutants F25R, E37A, and D74A lost the ability to induce Casp-8 activation (Fig. 6d, lanes 6, 18, and 22, respectively), these mutants permitted cFLIP$_L$-expression-induced Casp-8 activation (Fig. 6d, lanes 7, 19, and 23, respectively). Since the binary cFLIP-Casp-8 complex could recruit the inactive FADD F25G mutant (Fig. 5f), it is highly likely that the binary complex formed upon cFLIP$_L$ expression could also recruit

Casp-8 activation-defective FADD mutants F25R, E37A, and D74A to locally activate Casp-8. We further conducted a pulldown assay and confirmed that the purified binary complex could bind the His-tagged FADD D74A mutant (Supplementary Fig. 8c, lane 6). Taken together, these mutagenesis results not only underscore the distinct FADD surface requirements between hierarchical and reverse hierarchical binding processes but also emphasize the critical role of FADD in $cFLIP_L$-expression-induced Casp-8 activation. FADD residues K33 and E51 are indispensable for Casp-8 activation in both hierarchical and reverse hierarchical binding processes.

Added-FADD-induce RIPK1 activation is not inhibited by cFLIP

The addition of WT FADD, FADD mutants R34A, or D74A to HeLa cell lysate was previously shown to induce RIPK1 phosphorylation or activation, regardless of their ability to activate Casp-8[56], as evidenced in Fig. 6d, lanes 2, 10, and 22, respectively. This RIPK1 activation is likely facilitated by a distinct triple-FADD-Casp-8 complex, separate from the concurrently induced Casp-8-activating complex[56]. Notably, $cFLIP_L$ expression minimally affected RIPK1 phosphorylation induced by the addition of WT FADD or its mutants R34A and D74A (Fig. 6d, lanes 3 vs 2, 11 vs 10, and 23 vs 22, respectively), despite significantly reducing the Casp-8 activation induced by added-FADD (WT FADD and FADD R34A). Hence, the observed inconsistency in mutagenesis results supports the notion that added-FADD prompts the formation of two distinct complexes: a RIPK1-activating complex and a Casp-8-activating complex, with the latter susceptible to inhibition by cFLIP.

Furthermore, considering the earlier observation wherein increased cFLIP levels led to RIPK1 cleavage (Fig. 6b, lanes 3 and 15), it is evident that the ternary complex induced by cFLIP expression, resulting in RIPK1 cleavage and Casp-8 activation, differs from the RIPK1-activating complex prompted by added-FADD.

Since the regulation of caspase activation and RIPK1 cleavage is vital for controlling apoptosis and necroptosis, the findings presented in Fig. 6 highlight a significant connection between the reverse hierarchical binding process and these key regulatory pathways. The ability of tandem DED to orchestrate the assembly of a helical multiprotein DED complex in reverse order introduces an additional dimension of complexity to the intricate formation of this multiprotein DED complex (Fig. 7), ultimately influencing cell survival and fate. It is speculated that high levels of cFLIP in tumor cells could potentially overcome not only DR-induced death signaling but also stress-induced death signaling, thereby enhancing cell survival under adverse conditions.

Discussion

In summary, we investigate the tDED assembly of cFLIP in recruiting Casp-8. We present the atomic coordinates of the binary 6:4 CF^{H7G}-$C8^{FGLG}$ and 9:4 CF-$C8^{FGLG}$ complexes at 2.1 Å and 3.3 Å resolution, respectively (Figs. 1 and 2), unveiling the autonomous assembly of tDED between cFLIP and Casp-8 in the absence of FADD (Fig. 3). We also present the atomic coordinates of the ternary CF-$C8^{FuL\_FGLG\_CADA}$-FA^{FuL_F25G} complexes at 3.7 Å resolution (Fig. 5). Notably, these atomic coordinates reveal specific interactions within the cFLIP double-layer intermediate complex, which precedes the interaction with Casp-8 (Fig. 4 and Supplementary Fig. 4). In addition, they provide structural insights into specific binding of binary cFLIP-Casp-8 tDED complex to FADD, even the inactive FADD F25G mutant, leading to the release of cFLIP, Casp-8 activation, and RIPK1 cleavage (Figs. 5–7 and Supplementary Fig. 8). These findings suggest that the widely accepted hierarchical binding process[5] could occur in reverse order in vitro. Importantly, these structural revelations are pivotal for comprehending the role of cFLIP, particularly when its levels are elevated, in maintaining cell viability and influencing cellular immortality[47].

The appeal of this study lies in the discovery of a reverse hierarchical DED assembly, which contrasts both in hierarchy and directionality with the previously established unidirectional behavior of DD-fold proteins in filamentous complex assembly[68–72]. Unlike the unidirectional multiprotein DD-fold assemblies that align with downstream signaling hierarchies, our findings reveal that the FADD-Caspase-8-cFLIP DED assembly can occur in reverse order, forming a cFLIP-Caspase-8-FADD DED assembly. Additionally, we found that CBS formation could control the directionality of multiprotein DD-fold assembly. When the "type a" CBS appears on the oligomeric FADD-Caspase-8 intermediate complex, the subsequent DED assembly proceeds downstream by recruiting cFLIP. Conversely, when the "type b" CBS appears on the oligomeric cFLIP intermediate complex (Supplementary Fig. 3c), the DED assembly could proceed in reverse, binding first to Caspase-8 and then to FADD. The CBS on the cFLIP double layer for recruiting additional cFLIP is also composed of "type a" surfaces. This discrepancy in CBS composition and specificity dictates the directionality of complex elongation, contributing to the unidirectional nature of the assembly process. It is tempting to speculate that the co-occurrence of this reverse assembly of the cFLIP-Caspase-8-FADD complex under certain conditions may contribute to different models proposed in previous studies in this field and impact cell fate determination.

Notably, the recruitment of FADD to the binary cFLIP-Casp-8 complex, essential for expressed-cFLIP-induced Casp-8 activation in HeLa cell lysate (Fig. 6), leads to the displacement of cFLIP (Fig. 5), hinting at their interdependent assembly-function relationship. Comparing to the parental 9:4 CF-$C8^{FGLG}$ complex, FADD recruitment reduces the number of cFLIP molecules to five in the 5:3:3 CF-$C8^{FuL\_FGLG\_CADA}$-FA^{FuL_F25G} complex (Fig. 5), approaching the four cFLIP molecules in the 3:3:4 $FADD^{FuL}$-$C8^{FuL\_FGLG\_CADA}$-CF structure (PDB: 8YBX[56]), which likely represent the final product in the hierarchical binding process. Previously, our model predicted that the heterodimerization between procaspase-8 and the fourth $cFLIP_L$ molecule in the 3:3:4 $FADD^{FuL}$-$C8^{FuL\_FGLG\_CADA}$-CF structure would result in partial Casp-8 activation[56] (Fig. 7). Thus, in the reverse hierarchical binding process, the reduction in cFLIP molecules upon transitioning to the ternary cFLIP-Casp-8-FADD complex may trigger partial Casp-8 activation. A possible outcome is that the release of cFLIP eliminates the interference from neighboring pseudo-caspase domains or cFLIP, facilitating partial Casp-8 activation. However, the detailed mechanism requires future investigations.

The structural mechanism underlying the release of cFLIP upon FADD binding to the CF-$C8^{FGLG}$ complex could be investigated through structural comparison. By superimposing Casp-8 molecule C8c, a comparison between the ternary 3:3:4 $FADD^{FuL}$-$C8^{FuL\_FGLG\_CADA}$-CF (PDB: 8YBX[56]) and corresponding binary 9:4 CF-$C8^{FGLG}$ structures reveals that the bottom end WT cFLIP molecule CFh of the former shifts approximately 5 Å upon FADD joining the binary complex (Supplementary Fig. 9a). Similarly, a ~ 5 Å shift of the corresponding CF^{H7G} molecule CFh is also observed when comparing the ternary 1:5:4 $FADD^{FuL\_H9G}$-$C8^{FGLG}$-CF^{H7G} (PDB: 8YD8[56]) with corresponding binary 6:4 CF^{H7G}-$C8^{FGLG}$ structures (Supplementary Fig. 9b). Therefore, the release of cFLIP molecules during the transition to the ternary complex in the reverse hierarchical binding process is likely attributed to FADD-binding-induced structural jamming (Supplementary Movies 6 and 7).

In contrast, the FADD F25G mutation has minimal impact on the CF-$C8^{FGLG}$ assembly when comparing the ternary 5:3:3 CF-$C8^{FuL\_FGLG\_CADA}$-FA^{F25G} Complex C with the corresponding binary 8:3 CF-$C8^{FuL\_FGLG\_CADA}$ Complex F (Supplementary Fig. 9c). Consequently, the ineffective jamming observed in the FADD F25G mutant likely explains its inability to efficiently generate a C8-CF hetero-double layer, as seen with WT FADD in the ternary 3:3:4 $FADD^{FuL}$-$C8^{FuL\_FGLG\_CADA}$-CF complex (PDB: 8YBX[56]). Notably, since FADD residue F25 does not reside on the FADD-cFLIP and FADD-Casp-8 interfaces, there may be a correlation between the ineffective jamming caused by the FADD F25G mutant and its weak binding affinity toward Casp-8 and cFLIP[61,62]. This could result in the mutant's early dissociation from approximately 80% cryo-EM particles of the ternary complex, leading to the formation of various binary 8:3,

https://doi.org/10.1038/s41467-024-53306-1

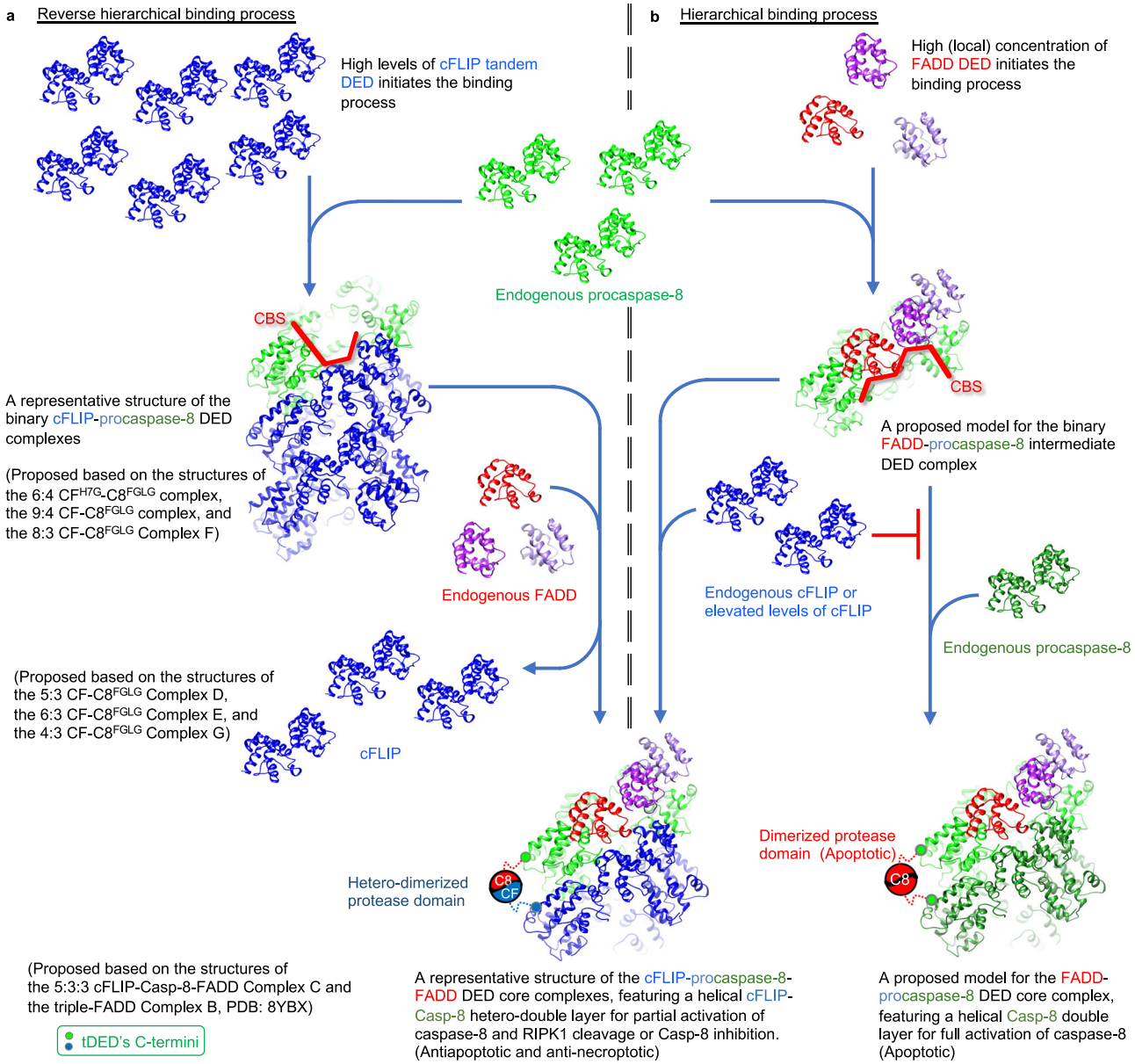

Fig. 7 | Proposed bidirectional DED assembly mechanisms in forming the ternary complex of cFLIP, FADD, and procaspase-8 in determining cell fate. **a** Proposed DED assembly mechanism in the reverse hierarchical binding process. When cFLIP levels are elevated, some cFLIP molecules could initiate the formation of a transient cFLIP double-layer intermediate complex. This intermediate complex recruits endogenous Casp-8 and cFLIP to form a stable binary complex. The resultant cFLIP-Casp-8 binary complex subsequently utilizes the CBS to recruit endogenous FADD and loses excess cFLIP molecule, resulting in a ternary cFLIP-Casp-8-FADD complex. This complex, similar to the one formed through the hierarchical binding process, provides resistance to apoptosis and necroptosis. Together with the hierarchical binding process shown in (**b**), the reverse hierarchical binding process completes the bidirectional DED assembly mechanism. **b** Proposed DED assembly mechanism in the hierarchical binding process[56]. Upon high levels of FADD or a high local concentration of FADD, FADD initiates the formation of a transient binary intermediate complex with endogenous Casp-8. cFLIP targets the CBS of this intermediate complex to block apoptotic signaling, resulting in a ternary FADD-Casp-8-cFLIP complex. When cFLIP is depleted, the intermediate complex could recruit endogenous procaspase-8 to initiate apoptosis. Blue and green ribbons represent cFLIP and Casp-8, respectively. FADD molecules are colored as their counterparts in Fig. 1d.

6:3, 5:3, and 4:3 complexes as byproducts. Future investigation is needed to elucidate the mechanical implications of the F25G mutation and the ineffectual jamming mechanically on the weak binding affinity of the FADD F25G mutant. It should also be noted that the byproducts of the binary complexes observed here may be absent in cells with WT FADD due to the completion of the transition.

Our structural studies do have certain limitations. Using Casp-8 FGLG and cFLIP H7G mutations, along with overexpression of cFLIP tDED, was intended to enhance sample homogeneity for structural studies[56]. The FADD F25G mutation was employed to bypass the hierarchical binding process and study the complex assembled in reverse order. Consequently, our structures may not fully represent the diverse native complexes found in cells. Additionally, the byproducts observed with the FADD F25G mutation are unlikely to be present in cells with WT FADD. Furthermore, the levels of cFLIP induced by cFLIP overexpression in our experiments may not mirror those induced by cell-type-specific TNF-induced RIPK1-mediated NF-κB activation[17,19–25], or TLR[49], or by various transcription factors[28,44], or in many tumor cells[7,28,44,73]. Depending on the levels of cFLIP and the equilibrium constant, it is conceivable that in these cells only a fraction of cFLIP could autonomously form the binary cFLIP-Casp-8 complex, which could then bind FADD to execute functions such as RIPK1

cleavage for maintaining cell viability[32,39] or even regulating autophagy[74] and the functions of inflammasomes[45,49]. These possibilities merit further investigations.

Additionally, it is possible that native binary complexes obtained from cells may exhibit heterogeneity, potentially containing more than one type III-II-III CSS-mediated Casp-8 trimer at the top end, each potentially serving distinct functions. Another scenario could involve the binary complex displaying a preference for binding endogenous FADD, resulting in the formation of heterogeneous ternary complexes. Consequently, the atomic coordinates of our binary complexes merely suggest potential interactions between cFLIP^{tDED}-cFLIP^{tDED} and cFLIP^{tDED}-Casp-8^{tDED} in the absence of FADD or before its recruitment. Furthermore, the atomic coordinates of the ternary complex, assembled in reverse order using the well-known inactive FADD F25G mutant, could provide insights into FADD's role in modulating the number of cFLIP molecules and its involvement in partial Casp-8 activation. Proposed ternary complex intermediates with WT FADD during the transition to the representative 3:3:4 FADD-C8-CF complex (PDB: 8YBX[56]) could be inferred from the structures detailed in our study (Fig. 7). These possibilities underscore the potential heterogeneity and intermediate states that require further exploration.

The structural insights from this study reveal previously unexplored FADD-independent assembly of the cFLIP^{tDED}-Casp-8^{tDED} complex and the subsequent recruitment of the FADD F25G mutant to form the ternary cFLIP^{tDED}-Casp-8^{tDED}-FADD^{DED} complex. These findings contribute another crucial piece to comprehensively understanding the intricate helical assembly of multiprotein DED/tDED complexes in three dimensions[75]. By revealing that elevated levels of cFLIP^{tDED} could potentially assemble a triple-layer helical complex via type III-II-III CSS-mediated trimer to initiate a reverse hierarchical binding process (as illustrated in Fig. 7a, with detailed steps in Supplementary Fig. 10), these findings provide a plausible explanation for previously controversial observations involving elevated levels of cFLIP in this field[29]. In conjunction with the hierarchical binding process in 3D[56], these results lay the structural foundation for the bidirectional, i.e., hierarchical and reverse hierarchical, DED assembly mechanisms in 3D, shedding light on the intricate signaling regulation by the helical FADD-Casp-8-cFLIP complexes of higher-order-assemblies (Fig. 7a, b). This work advances our understanding of the potential transitions leading to different higher-order DED/tDED complexes (detailed in Supplementary Fig. 10), which may play diverse signaling roles in cells[76] and contribute to the formation of punctate spots in tumor cells[47]. These findings underscore the need for further research to explore the functional implications embedded in these intricate structural discoveries. Future investigations should determine whether other helical multiprotein DD-fold complexes exhibit similar bidirectional assembly mechanisms.

This study's findings hold significant potential for advancing drug development aimed at treating cancers and inflammatory diseases. The atomic coordinates presented here could serve as crucial foundations for designing therapeutic strategies. For instance, a recent study highlighted the use of a peptide mimicking a helix of Caspase-8 DED2 to disrupt type I DED-DED interactions, successfully inhibiting apoptosis[77]. Similarly, another study used a homology-modeled cFLIP DED2 in in silico screening to identify inhibitors that could restore apoptosis in TRAIL-resistant cancer cells[78]. In this context, our structural data provide critical insights for the rational design of peptides or drugs that selectively target apoptotic complexes, such as the FADD-Caspase-8 intermediate complex[56], while avoiding anti-apoptotic complexes. Additionally, our structures presented here could inform drug screening efforts or guide the design of molecules that selectively target complexes assembled in reverse order, focusing on the DED-DED interactions used only in cFLIP double-layer formation or the Caspase-8-recruiting CBS of the cFLIP complex. This approach could selectively inhibit cFLIP self-oligomerization or its recruitment of Caspase-8, offering a promising strategy for treating cancers with elevated cFLIP levels, while preserving the integrity of apoptotic complexes. Moreover, targeting the FADD-recruiting CBS of the cFLIP-Caspase-8 complex presents another viable therapeutic avenue for such cancers.

Methods

Reconstitution and purification of the binary complex

To reconstitute the binary tDED complexes, wild-type or mutant cFLIP^{tDED} (1-181) proteins fused with an N-terminal 6xHis-tag (N-tag) and Casp-8^{tDED_FGLG} (1-185) mutant were individually expressed in *Escherichia coli* (BL21-CodonPlus, Agilent). The binary complexes were co-purified using Ni-nitrilotriacetic acid affinity resin followed by size-exclusion chromatography (SEC) employing a Superdex-200 (10/300) gel-filtration column (Cytiva) equilibrated with Buffer A (80 mM NaCl and 20 mM Tris, pH 8.0). The selenomethionine (SeMet, Carbosynth FS09881)-substituted protein complex was expressed and co-purified using the same method. The cloning primers are listed in Supplementary Data 1.

Crystallization of the binary complex

To crystallize the binary tDED complexes, the purified protein complexes underwent thrombin digestion to remove the N-terminal His-tag. Subsequently, they were concentrated and further purified using a Superdex-200 (10/300) gel-filtration column equilibrated with Buffer A. The native and SeMet-substituted CF^{H7G}-C8^{FGLG} complexes were concentrated to 20 mg/mL and crystallized using the hanging-drop vapor-diffusion method at 20 °C with a condition comprising 100 mM MES at pH 6.5, 200 mM KSCN, 80 mM NaCl, 10% PEG4000, and 10 mM TCEP at pH 7.3. Meanwhile, the CF-C8^{FGLG} complex was concentrated to 16 mg/mL and crystallized under conditions of 100 mM HEPES at pH 7.5, 100 mM LiCl, 100 mM TBG at pH 9.0, and 20% PEG400.

Reconstitution and purification of the ternary complex

To reconstitute the ternary DED complexes, wild-type cFLIP^{tDED} protein, full-length Casp-8^{FGLG_CADA} mutant, and full-length FADD F25G mutant fused with a His-tag were individually expressed in *Escherichia coli*. Ternary complexes were co-purified by using Ni-nitrilotriacetic acid affinity resin followed by size-exclusion chromatography (SEC) using a Superdex-200 (10/300) gel-filtration column equilibrated with Buffer A. The purified complex protein was then subject to cross-linking, as described in the corresponding section below.

The generation of the ternary DED complex with FADD F25Y mutant is depicted in Fig. 5a. In this process, the His-tag-removed, SEC-purified binary CF^{H7G}-C8^{FGLG} complex was added to FADD^{Ful_F25Y}-loaded resin at 4 °C for 1 h. The eluted protein was then subject to SEC using a Superdex-200 (10/300) gel-filtration column equilibrated with Buffer A. Subsequently, the purified complex protein underwent negative stain EM studies described in the corresponding section below.

Crystal structure determination and molecular graphics

Anomalous and native diffraction data were collected X-ray by the program Blu-Ice 5.0 at the TLS BL13B1 beamline at NSRRC, using the wavelengths of 0.97942 and 1.00000 Å, respectively, at 110 K. The data sets underwent processing using the HKL-3000 program. The CF^{H7G}-C8^{FGLG} structure was determined at 2.34 Å using the single-wavelength anomalous diffraction (SAD) phasing in the Phenix software (version 1.14-3260), with Se atoms serving as anomalous scatterers. Within the asymmetric unit, there was one 6:4 CF^{H7G}-C8^{FGLG} complex, with a solvent content of 55%. The CF-C8^{FGLG} structure was determined using the molecular replacement (MR) method, utilizing the CF^{H7G}-C8^{FGLG} structure as a search model and the Phaser-MR GUI in Phenix version 1.14-3260. Within the asymmetric unit, there was one 9:4 CF-C8^{FGLG} complex, with a solvent content of 65%. The identification of Casp-8 and cFLIP was based on the selenium atom positions. Consistent with our previous findings[56], there are electron

densities for helix H7 of Casp-8 and cFLIP tDEDs, while cFLIP has disordered helix H3 in DED1 and sometimes DED2 (Supplementary Fig. 1a, b).

All models underwent iteratively building and refinement processes using the programs Coot version 0.8.9.1 EL/WinCoot version 0.8.2 and Phenix version 1.14-3260, respectively. In both structures, all residues fell within the Ramachandran favored and allowed regions, with no outliers. Data collection and refinement statistics are summarized in Supplementary Table 1. The structures were analyzed using the qtPISA program in CCP4i2 version 7.0.060, MUSTANG version 3.2.3, and Mol-Probity (http://kinemage.biochem.duke.edu). Interface residues and areas were identified and estimated, respectively, by PISA. Figures were prepared using the PyMOL version 1.8.2.1 and UCSF Chimera programs version 1.16-42360. Movies were prepared using UCSF Chimera programs version 1.16-42360 and UCSF ChimeraX version 1.6.dev202303040240.

The ball-and-ribbon diagram

In Fig. 2c, the ball-and-ribbon diagram on the right-hand side illustrates the spatial relationship of individual DEDs within the CF-C8^{FGLG} complex. Lines connect the spatially conserved Cα atoms of every two adjacent DEDs, forming ribbons that represent the assemblies via the type I, II, and III interfaces, respectively. Blue, green, and cyan ribbons denote assemblies through the type I interface (referred to as the type I connectivity), while gray ribbons indicate assemblies via the type II interface (the type II connectivity). Red, yellow, and pink ribbons represent assemblies through the type III interface (the type III connectivity). The balls represent the Cα atoms of spatially conserved leucine residues of DEDs[56], including Casp-8 L62 and L162, and cFLIP L55 and L152. This diagram was made by using the PyMOL program version 1.8.2.1

Multi-angle light scattering (MALS)

In the SEC-MALS experiments, binary and ternary DED complexes were injected into a Superdex 200 (5/150) size-exclusion column and a Wyatt protein SEC column with a pore size of 300 Å, respectively. All columns were equilibrated with 20 mM Tris (pH 8.0) and 80 mM NaCl at room temperature, using a fast protein liquid chromatography system (Äkta purifier 10) coupled with a three-angle light-scattering detector (mini-DAWN TREOS) and a refractive index detector (Optilab T-rEX, Wyatt Technology). Data analysis was carried out using the program ASTRA ver 6.0.5.3.

Small-angle X-ray scattering

In the SEC-SAXS experiments, SAXS data were collected using the program Albula (Dectris, Baden-Dättwil, Switzerland) at the SWAXS beamline BL23A1 at NSRRC using an online size-exclusion high-performance liquid chromatographic system (Agilent chromatographic system 1260 series). Each protein sample was injected into an Agilent Bio SEC-5 HPLC column with a flow rate of 0.35 mL/min. Upon elution of the complex, the solution passed through a quartz capillary (2.0 mm diameter) with a flow rate decreased to 0.03 mL/min for the SAXS data collected with 30 s per frame using a Pilatus 1M-F area detector. All buffer solutions were measured under the same conditions for background scattering subtraction. The SAXS data were analyzed using BioXTAS RAW 2.2.2 and the ATSAS program suite version 2.7 to 3.2.1. Data collection and structural parameters are summarized in Supplementary Table 2.

Negative staining TEM

Four µl of the sample solution was applied onto the carbon-coated side of a TEM carbon type-B grid (Ted Pella, 01814-F) for 30 s, followed by the removal of excess liquid from the edge of grid using a filter paper (Whatman). Subsequently, 4 µl of 1% uranyl acetate or uranyl formate was applied to the grid for 30 s and then removed with a filter paper. The grid was then placed into an electronic dry cabinet to air dry before imaging using a FEI Tecnai G2 F20 S-TWIN at ICOB, Academia Sinica. Uncropped data are included in a Source Data file.

Protein sample cross-linking

Before cross-linking, purified protein complexes were dialyzed against a HEPES buffer and then concentrated to 1 mg/mL. For Bis-sulfosuccinimidyl suberate (BS3) cross-linking, 12.5 mM BS3 was added to 1 mL of purified protein to achieve a final BS3 concentration of 2.5 mM, and the mixture was allowed to react at room temperature for an hour. Subsequently, the reaction mixture was then loaded onto a size-exclusion chromatography column (Superdex 200 increase 10/300), and equilibrated in a TRIS buffer, to remove excess BS3. The peak fractions were collected and stored at 4 °C. The concentration of the cross-linked complex was measured using a spectrophotometer (NanoDrop ND-1000, Thermo Scientific) prior to grid preparation.

Cryo-EM grids preparation and data acquisition

The BS3 cross-linked protein samples (approximately 250 µg/mL of the complexes C to G) were applied to glow-discharged holey carbon grids (Quantifoil Cu, R1.2/1.3, 300 mesh). Each grid was blotted for 3 to 4 s and then flash-plunged into liquid ethane pre-cooled in liquid nitrogen using an FEI Vitrobot mark IV operated at 4 °C and 100% humidity. Cryo-EM data were acquired on a Titan Krios (FEI) operated at 300 kV, equipped with a Gatan K2 Summit detector at ASCEM, Academia Sinica. The EPU 2.2.0.65REL software was utilized for automated data collection. Movies were collected at a nominal magnification of 165,000× in counting mode resulting in a calibrated pixel size of 0.84 Å/pixel, with a defocus range of approximately −1.0 to −1.6 µm. Eighty frames were recorded over 6 s of exposure at a dose rate of 0.9 electrons per Å^2 per frame. Data collection, refinement, and validation statistics are summarized in Supplementary Table 3.

Cryo-EM image processing and model refinement

All datasets underwent processing using the CryoSparc V2.8.0 to V2.11.0 software package installed on our own computers. Movie frames were aligned by executing the Full-frame motion correction job. The contrast transfer function parameters for each aligned micrograph were estimated using CTF estimation (CTFFIND4). Particle templates were created from the manually picked particles from 15 ~ 20 micrographs. Subsequently, particles were automatically picked using the Template picker tool. All particles were locally aligned and extracted by employing Local motion correction, followed by multiple cycles of 2D classification to remove junk particles. Ab initio 3D classification was conducted using the Ab-initio Reconstruction module. After discarding junk particles, subsequent procedures including heterogeneous refinement, homogeneous-refinement, and non-uniform refinement were carried out. All map structures were sharpened, and the resolution was estimated using the Fourier shell correlation (FSC) = 0.143 cutoff criterion.

The crystal structures of FADD^{DED}, cFLIP^{tDED}, and C8^{tDED} were fitted into the Cryo-EM envelops using UCSF Chimera version 1.16-42360 and refined in real space using the Phenix version 1.14-3260. The identification of Casp-8 and cFLIP was facilitated by the presence of envelops for helix H7 of tDED, with further confirmation of cFLIP identity through the observation of disordered helix H3 in cFLIP DED1 and sometimes DED2[56]. Maps for each helix with structural model are shown in Supplementary Figs. 11–15. Notably, given that tDED but not FADD DED possesses helix H7, the absence of an envelope for helix H7 of tDED distinctly indicates the presence of three FADD DED molecules in Complex C (Supplementary Fig. 7a vs b, and Supplementary Fig. 11). Notably, the Casp-8's caspase domain and FADD DD were not visible in the Cryo-EM envelopes.

Mutagenesis and pulldown assays

All gene mutations were introduced using the KOD Plus Mutagenesis Kit (TOYOBO) or the In-Fusion HD Cloning Plus kit (TaKaRa). The

primers used in mutagenesis are listed in Supplementary Data 1. The His-tagged proteins were expressed and immobilized on resin (Qiagen). Excess proteins and impurities were removed by three washes with 40 mM imidazole. The resin was then incubated with non-tagged protein lysates at room temperature for 1 h, followed by three washes with 40 mM imidazole. Finally, the proteins were eluted with 1 M imidazole. All samples underwent SDS-PAGE analysis with Coomassie blue staining. The representative images from two independent experiments are shown. Bar charts in Fig. 4c and Supplementary Fig. 4c were made by Excel version 16.54. Uncropped data are included in a Source Data file.

In vitro mutagenesis study of FADD-mediated signaling

In vitro mutagenesis experiments were performed using a HeLa cell lysate-based protein expression system (1-Step Human Coupled IVT kit, Thermo). The full-length cFLIP and cFLIP^{tDED} cDNA sequences were cloned into the pT7CFE1-CHis expression vector for human cell-free protein expression. Full-length wild type and mutant FADD proteins were expressed using the PURExpress in vitro protein synthesis kit (NEB) with the pET-26 vector. For cFLIP protein expression, the cFLIP construct was mixed with the reaction component of the IVT kit and incubated at 30 °C for 16 or 32 h. Different FADD proteins were added at the time point 0 h or 16 h to a final concentration of approximately 4 μM (measured by UV absorbance), which is higher than the endogenous FADD concentration of approximately 0.33 μM[79]. The in vitro reaction product was subsequently analyzed by SDS-PAGE and western blotting. Mutants were created using KOD-based site-directed mutagenesis and the primers listed in Supplementary Data 1. Uncropped data are included in a Source Data file.

Western blotting

Cell lysates containing 20 μg of protein were subjected to SDS-PAGE analysis and subsequently transferred to a PVDF membrane (Millipore). The membrane was then blocked with a Tris-buffered saline containing 0.1% Tween-20 (TBST), supplemented with either 5% (wt/vol) skim milk or 1% BSA, for one hour at room temperature. Following blocking, the membrane was washed three times with TBST to remove excess blocking reagent. Next, the blot was incubated with the indicated primary antibodies at 4 °C overnight, followed by another three washes with TBST. Afterward, the membrane was incubated with HRP-conjugated secondary antibodies for one hour at room temperature. To visualize the protein bands, the blot was washed four times with TBST and then treated with the ECL solution (Pierce) following the manufacturer's instructions. Representative images of two independent experiments are presented. Uncropped data are included in a Source Data file.

Antibodies used in the cell-lysate based experiments

FLIP (D5J1E) (Cell Signaling, #56343, 1:2000); Caspase 8(D35G2) (Cell Signaling, #4790, 1:4000); Caspase-3 antibody (Cell Signaling, #9662, 1:4000); Cleaved caspase-3 (Asp175) (5A1E) (Cell Signaling, #9664, 1:2000); Human FADD (Cell Signaling, #2782, 1:2000); PARP (46D11) (Cell Signaling, #9532,1:2000); RIP (Cell Signaling, #4926, 1:2000); Phospho-RIP (Ser166) (D1L3S) (Cell Signaling, #65746, 1:2000); GAPDH (14C10) (HRP Conjugate) (Cell Signaling, #3683, 1:4000); Goat Anti-Rabbit IgG H&L (HRP) (Abcam, #ab6721, 1:10000)

Reporting summary

Further information on research design is available in the Nature Portfolio Reporting Summary linked to this article.

Data availability

The atomic coordinates and reflection files for the crystal structures generated in this study have been deposited in the Worldwide Protein Data Bank (wwPDB) under accession codes 8YM4 (The SeMet derivative of the CF^{H7G}-C8^{FGLG} complex), 8YM5 (Native CF^{H7G}-C8^{FGLG} complex), and 8YM6 (Native CF-C8^{FGLG} complex). The cryo-EM structures and the corresponding atomic coordinates generated in this study have been deposited in the Electron Microscopy Data Bank (EMDB) and wwPDB, respectively, under accession codes EMD-39424 and 8YNI (The 5:3:3 CF-C8^{FuL_FGLG_CADA}-FA^{FuL_F25G} DED Complex C), EMD-39425 and 8YNK (The 5:3 CF-C8^{FGLG} Complex D), EMD-39426 and 8YNL (The 6:3 CF-C8^{FGLG} Complex E), EMD-39427 and 8YNM (The 8:3 CF-C8^{FGLG} Complex F), and EMD-39428 and 8YNN (The 4:3 CF-C8^{FGLG} Complex G). The cryo-EM structure used in this study are available in the EMDB under accession codes EMD-39126 (The triple-FADD-Casp-8-cFLIP DED Complex B)[56]. The atomic coordinates for the cryo-EM structure used in this study are available in the wwPDB under accession codes 8YBX (The triple-FADD-Casp-8-cFLIP DED complex B)[56], and 8YD8 (Native single-FADD-Casp-8-cFLIP DED complex)[56]. The atomic coordinates for the NMR structure used in this study are available in the wwPDB under accession codes 2GF5 (Full-length FADD)[63]. The SDS-PAGE data, western blot data, representative micrographs, and other source data generated in this study are provided in the Supplementary Information or in a Source Data file. Source data are provided as a Source Data file. Source data are provided with this paper.

References

1. Tang, D., Kang, R., Berghe, T. V., Vandenabeele, P. & Kroemer, G. The molecular machinery of regulated cell death. *Cell Res* **29**, 347–364 (2019).
2. Singh, R., Letai, A. & Sarosiek, K. Regulation of apoptosis in health and disease: the balancing act of BCL-2 family proteins. *Nat. Rev. Mol. Cell Biol.* **20**, 175–193 (2019).
3. Peter, M. E. et al. The CD95 receptor: apoptosis revisited. *Cell* **129**, 447–450 (2007).
4. Wilson, N. S., Dixit, V. & Ashkenazi, A. Death receptor signal transducers: nodes of coordination in immune signaling networks. *Nat. Immunol.* **10**, 348–355 (2009).
5. Hughes, M. A. et al. Co-operative and hierarchical binding of c-FLIP and caspase-8: a unified model defines how c-FLIP isoforms differentially control cell fate. *Mol. Cell* **61**, 834–849 (2016).
6. Kischkel, F. C. et al. Cytotoxicity-dependent APO-1 (Fas/CD95)-associated proteins form a death-inducing signaling complex (DISC) with the receptor. *EMBO J.* **14**, 5579–5588 (1995).
7. Irmler, M. et al. Inhibition of death receptor signals by cellular FLIP. *Nature* **388**, 190–195 (1997).
8. Rasper, D. M. et al. Cell death attenuation by 'Usurpin', a mammalian DED-caspase homologue that precludes caspase-8 recruitment and activation by the CD-95 (Fas, APO-1) receptor complex. *Cell Death Differ.* **5**, 271–288 (1998).
9. Scaffidi, C. et al. Differential modulation of apoptosis sensitivity in CD95 type I and type II cells. *J. Biol. Chem.* **274**, 22532–22538 (1999).
10. Scaffidi, C., Schmitz, I., Krammer, P. H. & Peter, M. E. The role of c-FLIP in modulation of CD95-induced apoptosis. *J. Biol. Chem.* **274**, 1541–1548 (1999).
11. Peter, M. E. & Krammer, P. H. The CD95(APO-1/Fas) DISC and beyond. *Cell Death Differ.* **10**, 26–35 (2003).
12. Lavrik, I. N. et al. CD95 stimulation results in the formation of a novel death effector domain protein-containing complex. *J. Biol. Chem.* **283**, 26401–26408 (2008).
13. Brenner, D., Blaser, H. & Mak, T. W. Regulation of tumour necrosis factor signalling: live or let die. *Nat. Rev. Immunol.* **15**, 362–374 (2015).
14. Hsu, H., Huang, J., Shu, H. B., Baichwal, V. & Goeddel, D. V. TNF-dependent recruitment of the protein kinase RIP to the TNF receptor-1 signaling complex. *Immunity* **4**, 387–396 (1996).
15. Shu, H. B., Takeuchi, M. & Goeddel, D. V. The tumor necrosis factor receptor 2 signal transducers TRAF2 and c-IAP1 are components of the tumor necrosis factor receptor 1 signaling complex. *Proc. Natl Acad. Sci. USA* **93**, 13973–13978 (1996).

16. Hsu, H., Xiong, J. & Goeddel, D. V. The TNF receptor 1-associated protein TRADD signals cell death and NF-kappa B activation. *Cell* **81**, 495–504 (1995).
17. Liu, Z. G., Hsu, H., Goeddel, D. V. & Karin, M. Dissection of TNF receptor 1 effector functions: JNK activation is not linked to apoptosis while NF-kappaB activation prevents. *Cell death. Cell* **87**, 565–576 (1996).
18. Hsu, H., Shu, H. B., Pan, M. G. & Goeddel, D. V. TRADD-TRAF2 and TRADD-FADD interactions define two distinct TNF receptor 1 signal transduction pathways. *Cell* **84**, 299–308 (1996).
19. Micheau, O. & Tschopp, J. Induction of TNF receptor I-mediated apoptosis via two sequential signaling complexes. *Cell* **114**, 181–190 (2003).
20. Varfolomeev, E. E. & Ashkenazi, A. Tumor necrosis factor: an apoptosis JuNKie? *Cell* **116**, 491–497 (2004).
21. Karin, M. & Lin, A. NF-kappaB at the crossroads of life and death. *Nat. Immunol.* **3**, 221–227 (2002).
22. Beg, A. A. & Baltimore, D. An essential role for NF-kappaB in preventing TNF-alpha-induced cell death. *Science* **274**, 782–784 (1996).
23. Van Antwerp, D. J., Martin, S. J., Kafri, T., Green, D. R. & Verma, I. M. Suppression of TNF-alpha-induced apoptosis by NF-kappaB. *Science* **274**, 787–789 (1996).
24. Micheau, O., Lens, S., Gaide, O., Alevizopoulos, K. & Tschopp, J. NF-kappaB signals induce the expression of c-FLIP. *Mol. Cell Biol.* **21**, 5299–5305 (2001).
25. Kreuz, S., Siegmund, D., Scheurich, P. & Wajant, H. NF-kappaB inducers upregulate cFLIP, a cycloheximide-sensitive inhibitor of death receptor signaling. *Mol. Cell Biol.* **21**, 3964–3973 (2001).
26. Harper, N., Hughes, M., MacFarlane, M. & Cohen, G. M. Fas-associated death domain protein and caspase-8 are not recruited to the tumor necrosis factor receptor 1 signaling complex during tumor necrosis factor-induced apoptosis. *J. Biol. Chem.* **278**, 25534–25541 (2003).
27. Wang, L., Du, F. & Wang, X. TNF-alpha induces two distinct caspase-8 activation pathways. *Cell* **133**, 693–703 (2008).
28. Safa, A. R. Roles of c-FLIP in Apoptosis, Necroptosis, and Autophagy. *J Carcinog Mutagen* **Suppl 6**, https://doi.org/10.4172/2157-2518.S6-003 (2013).
29. Tsuchiya, Y., Nakabayashi, O. & Nakano, H. FLIP the switch: regulation of apoptosis and necroptosis by cFLIP. *Int J. Mol. Sci.* **16**, 30321–30341 (2015).
30. Krueger, A., Schmitz, I., Baumann, S., Krammer, P. H. & Kirchhoff, S. Cellular FLICE-inhibitory protein splice variants inhibit different steps of caspase-8 activation at the CD95 death-inducing signaling complex. *J. Biol. Chem.* **276**, 20633–20640 (2001).
31. Krueger, A., Baumann, S., Krammer, P. H. & Kirchhoff, S. FLICE-inhibitory proteins: regulators of death receptor-mediated apoptosis. *Mol. Cell Biol.* **21**, 8247–8254 (2001).
32. Oberst, A. et al. Catalytic activity of the caspase-8-FLIP(L) complex inhibits RIPK3-dependent necrosis. *Nature* **471**, 363–367 (2011).
33. Holler, N. et al. Fas triggers an alternative, caspase-8-independent cell death pathway using the kinase RIP as effector molecule. *Nat. Immunol.* **1**, 489–495 (2000).
34. Chan, F. K. et al. A role for tumor necrosis factor receptor-2 and receptor-interacting protein in programmed necrosis and antiviral responses. *J. Biol. Chem.* **278**, 51613–51621 (2003).
35. Yeh, W. C. et al. Requirement for Casper (c-FLIP) in regulation of death receptor-induced apoptosis and embryonic development. *Immunity* **12**, 633–642 (2000).
36. Varfolomeev, E. E. et al. Targeted disruption of the mouse Caspase 8 gene ablates cell death induction by the TNF receptors, Fas/Apo1, and DR3 and is lethal prenatally. *Immunity* **9**, 267–276 (1998).
37. Yeh, W. C. et al. FADD: essential for embryo development and signaling from some, but not all, inducers of apoptosis. *Science* **279**, 1954–1958 (1998).
38. Li, J. et al. The RIP1/RIP3 necrosome forms a functional amyloid signaling complex required for programmed necrosis. *Cell* **150**, 339–350 (2012).
39. Dillon, C. P. et al. Survival function of the FADD-CASPASE-8-cFLIP(L) complex. *Cell Rep.* **1**, 401–407 (2012).
40. Kaiser, W. J. et al. RIP3 mediates the embryonic lethality of caspase-8-deficient mice. *Nature* **471**, 368–372 (2011).
41. Dillon, C. P. et al. RIPK1 blocks early postnatal lethality mediated by caspase-8 and RIPK3. *Cell* **157**, 1189–1202 (2014).
42. Dannappel, M. et al. RIPK1 maintains epithelial homeostasis by inhibiting apoptosis and necroptosis. *Nature* **513**, 90–94 (2014).
43. Gurung, P. et al. FADD and caspase-8 mediate priming and activation of the canonical and noncanonical Nlrp3 inflammasomes. *J. Immunol.* **192**, 1835–1846 (2014).
44. Humphreys, L., Espona-Fiedler, M. & Longley, D. B. FLIP as a therapeutic target in cancer. *Febs J.* **285**, 4104–4123 (2018).
45. Wu, Y. H. et al. Participation of c-FLIP in NLRP3 and AIM2 inflammasome activation. *Cell Death Differ.* **21**, 451–461 (2014).
46. Ranjan, K. & Pathak, C. FADD regulates NF-kappaB activation and promotes ubiquitination of cFLIPL to induce apoptosis. *Sci. Rep.* **6**, 22787 (2016).
47. French, R., Hayward, O., Jones, S., Yang, W. & Clarkson, R. Cytoplasmic levels of cFLIP determine a broad susceptibility of breast cancer stem/progenitor-like cells to TRAIL. *Mol. Cancer* **14**, 209 (2015).
48. Micheau, O. Cellular FLICE-inhibitory protein: an attractive therapeutic target? *Expert Opin. Ther. Targets* **7**, 559–573 (2003).
49. Van Opdenbosch, N. et al. Caspase-1 engagement and TLR-induced c-fLIP expression suppress ASC/Caspase-8-dependent apoptosis by inflammasome sensors NLRP1b and NLRC4. *Cell Rep.* **21**, 3427–3444 (2017).
50. Majkut, J. et al. Differential affinity of FLIP and procaspase 8 for FADD's DED binding surfaces regulates DISC assembly. *Nat. Commun.* **5**, 3350 (2014).
51. Fu, T. M. et al. Cryo-EM structure of caspase-8 tandem DED filament reveals assembly and regulation mechanisms of the death-inducing signaling complex. *Mol. Cell* **64**, 236–250 (2016).
52. Schleich, K. et al. Stoichiometry of the CD95 death-inducing signaling complex: experimental and modeling evidence for a death effector domain chain model. *Mol. Cell* **47**, 306–319 (2012).
53. Dickens, L. S. et al. A death effector domain chain DISC model reveals a crucial role for caspase-8 chain assembly in mediating apoptotic cell death. *Mol. Cell* **47**, 291–305 (2012).
54. Humphreys, L. M. et al. A revised model of TRAIL-R2 DISC assembly explains how FLIP(L) can inhibit or promote apoptosis. *EMBO Rep.* **21**, e49254 (2020).
55. Fox, J. L. et al. Cryo-EM structural analysis of FADD:Caspase-8 complexes defines the catalytic dimer architecture for co-ordinated control of cell fate. *Nat. Commun.* **12**, 819 (2021).
56. Yang, C. Y. et al. Deciphering DED assembly mechanisms in FADD-procaspase-8-cFLIP complexes regulating apoptosis. *Nat. Commun.* **15**, 3791 (2024).
57. Esposito, D. et al. Solution NMR investigation of the CD95/FADD homotypic death domain complex suggests lack of engagement of the CD95 C terminus. *Structure* **18**, 1378–1390 (2010).
58. Nematollahi, L. A. et al. Flexible stoichiometry and asymmetry of the PIDDosome core complex by heteronuclear NMR spectroscopy and mass spectrometry. *J. Mol. Biol.* **427**, 737–752 (2015).
59. Su, T. W. et al. Structural insights into DD-fold assembly and caspase-9 activation by the Apaf-1 apoptosome. *Structure* **25**, 407–420 (2017).

60. Lin, S. C., Lo, Y. C. & Wu, H. Helical assembly in the MyD88-IRAK4-IRAK2 complex in TLR/IL-1R signalling. *Nature* **465**, 885–890 (2010).
61. Eberstadt, M. et al. NMR structure and mutagenesis of the FADD (Mort1) death-effector domain. *Nature* **392**, 941–945 (1998).
62. Kaufmann, M. et al. Identification of a basic surface area of the FADD death effector domain critical for apoptotic signaling. *FEBS Lett.* **527**, 250–254 (2002).
63. Carrington, P. E. et al. The structure of FADD and its mode of interaction with procaspase-8. *Mol. Cell* **22**, 599–610 (2006).
64. Tsai, M. D., Wu, W. J. & Ho, M. C. Enzymology and dynamics by cryogenic electron microscopy. *Annu Rev. Biophys.* **51**, 19–38 (2022).
65. Yu, J. W., Jeffrey, P. D. & Shi, Y. Mechanism of procaspase-8 activation by c-FLIPL. *Proc. Natl Acad. Sci. USA* **106**, 8169–8174 (2009).
66. Pop, C. et al. FLIP(L) induces caspase 8 activity in the absence of interdomain caspase 8 cleavage and alters substrate specificity. *Biochem J.* **433**, 447–457 (2011).
67. Boatright, K. M., Deis, C., Denault, J. B., Sutherlin, D. P. & Salvesen, G. S. Activation of caspases-8 and -10 by FLIP(L). *Biochem J.* **382**, 651–657 (2004).
68. Hochheiser, I. V. et al. Directionality of PYD filament growth determined by the transition of NLRP3 nucleation seeds to ASC elongation. *Sci. Adv.* **8**, eabn7583 (2022).
69. Lu, A. et al. Unified polymerization mechanism for the assembly of ASC-dependent inflammasomes. *Cell* **156**, 1193–1206 (2014).
70. Li, Y. et al. Cryo-EM structures of ASC and NLRC4 CARD filaments reveal a unified mechanism of nucleation and activation of caspase-1. *Proc. Natl Acad. Sci. USA* **115**, 10845–10852 (2018).
71. Shen, C. et al. Molecular mechanism for NLRP6 inflammasome assembly and activation. *Proc. Natl Acad. Sci. USA* **116**, 2052–2057 (2019).
72. Schlauderer, F. et al. Molecular architecture and regulation of BCL10-MALT1 filaments. *Nat. Commun.* **9**, 4041 (2018).
73. Safa, A. R., Kamocki, K., Saadatzadeh, M. R. & Bijangi-Vishehsaraei, K. c-FLIP, a Novel biomarker for cancer prognosis, immunosuppression, alzheimer's disease, chronic obstructive pulmonary disease (copd), and a rationale therapeutic target. *Biomark J.* **5**, https://doi.org/10.36648/2472-1646.5.1.59 (2019).
74. Lee, J. S. et al. FLIP-mediated autophagy regulation in cell death control. *Nat. Cell Biol.* **11**, 1355–1362 (2009).
75. Lo, Y. C., Lin, S. C., Yang, C. Y. & Tung, J. Y. Tandem DEDs and CARDs suggest novel mechanisms of signaling complex assembly. *Apoptosis* **20**, 124–135 (2015).
76. Wu, H. Higher-order assemblies in a new paradigm of signal transduction. *Cell* **153**, 287–292 (2013).
77. Konig, C. et al. Targeting type I DED interactions at the DED filament serves as a sensitive switch for cell fate decisions. *Cell Chem. Biol.* https://doi.org/10.1016/j.chembiol.2024.06.014 (2024).
78. Yaacoub, K. et al. The identification of new c-flip inhibitors for restoring apoptosis in trail-resistant cancer cells. *Curr. Issues Mol. Biol.* **46**, 710–728 (2024).
79. Laussmann, M. A. et al. Proteasome inhibition can impair caspase-8 activation upon submaximal stimulation of apoptotic tumor necrosis factor-related apoptosis inducing ligand (TRAIL) signaling. *J. Biol. Chem.* **287**, 14402–14411 (2012).

Acknowledgements

This work was supported by Academia Sinica (AS) Thematic Program (AS-TP-107-L16, AS-TP-107-L16-1, AS-102-TP-B14 and AS-102-TP-B14-2 to S.-C.L.; AS-TP-107-L16-2 and AS-102-TP-B14-1 to Y.-C.L; AS-TP-107-L16-3 to L.-C.H.; AS Postdoc Fellowships to C.-Y.Y. and T.-W.S.), Ministry of Science and Technology (MoST) (MoST 107-2320-B-001-018-, 108-2311-B-001-018-, 109-2311-B-001-016-, and 110-2311-B-001-015- to S.-C.L.; MoST 107-2320-B-006-062-MY3, and 111-2311-B-006-005-MY3 to Y.-C.L.), and Taiwan Protein Project (TPP) (Grant No. AS-KPQ-105-TPP to Y.-C.L and S.-C.L.). We thank the Protein X-ray Diffractometer, Chameleon, and Vitrobot facilities of GRC for crystallization screening and sample preparation for cryo-EM, DNA Sequencing Core Facility of IBMS (AS CFII Project AS-CFII-113-A12) for DNA sequencing, AS Biological EM Core Facility of ICOB (AS-CFII-111-203) for negative stain EM data, AS Cryo-EM Facility (ASCEM) (AS-CFII-111-210 and TPP AS-KPQ-109-TPP2) for cryo-EM data. We thank the beamline BL13B1 and BL23A1 at NSRRC, Taiwan, for X-ray diffraction and SAXS data, respectively. We thank Prof. Ming-Daw Tsai, Prof. Chih-Hao Lee, Prof. Andrew Hui-Jun Wang, and Prof. Tien-Hsien Chang for their insightful feedback.

Author contributions

C.-Y.Y. expressed, purified, and crystallized the complexes, collected the SAXS, X-ray, and cryo-EM data, solved the structures, obtained the atomic coordinates, and made figures. Y.-C.T. did the cell lysate-based experiments. Y.-F.T. and Y.-C.T. did the pulldown experiments. C.-Y.Y., B.-J.K., Y.-C.T., Y.-F.T., C.-I.L., Y.-S.L., T.-W.S., and Y.-T.W. helped with data analysis and source data preparation. Y.-F.T., C.-Y.Y., Y.-C.T., Y.-T.W., Y.-C.Lu, and C.-I.L. made the constructs. S.-C.L., Y.-C.Lo., and L.-C.H. supervised the project and revised the manuscript. S.-C.L. and Y.-C.Lo analyzed and interpreted the data, made the final figures, and wrote the manuscript. S.-C.L. initiated the project.

Competing interests

The authors declare no competing interests.

Additional information

Supplementary information The online version contains supplementary material available at https://doi.org/10.1038/s41467-024-53306-1.

Correspondence and requests for materials should be addressed to Yu-Chih Lo or Su-Chang Lin.

Peer review information *Nature Communications* thanks Hyun Ho Park and the other, anonymous, reviewers for their contribution to the peer review of this work. A peer review file is available.